Key Points:
- Deglaciation in the Bering Sea was characterized by significant changes in sediment delivery, circulation, and productivity
- The Last Glacial Maximum and Early Deglacial are both heavily influenced by terrestrial sedimentation in the Bering Sea
- Sea level rise, decreasing sea ice, and increasing stratification led to high productivity during the Bølling-Allerød and Pre-Boreal

Supporting Information:
- Supporting Information S1

Correspondence to:
B. M. Pelto,
pelto@unbc.ca

Oceanographic and Climatic Change in the Bering Sea, Last Glacial Maximum to Holocene

Ben M. Pelto[1,2] (iD), **Beth E. Caissie**[3] (iD), **Steven T. Petsch**[2], and **Julie Brigham-Grette**[2]

[1]Natural Resources and Environmental Studies Institute and Geography Program, University of Northern British Columbia, Prince George, British Columbia, Canada, [2]Department of Geosciences, University of Massachusetts Amherst, Amherst, MA, USA, [3]Department of Geological and Atmospheric Sciences, Iowa State University, Ames, IA, USA

Abstract Post-glacial sea level rise led to a direct connection between the Arctic and Pacific Oceans via the Bering Strait. Consequently, the Bering Sea experienced changes in connectivity, size, and sediment sources that were among the most drastic of any ocean basin in the past 30,000 years. However, the sedimentary response to the interplay between climate change and sea level rise in high-latitude settings such as Beringia remains poorly resolved. To ascertain changes in sediment delivery, productivity, and regional oceanography from the Last Glacial Maximum (LGM) to the Holocene, we analyzed sedimentological, geochemical, and isotopic characteristics of three sediment cores from the Bering Sea. Interpretations of productivity, terrestrial input, nutrient utilization, and circulation are based on organic carbon isotopes ($\delta^{13}C_{org}$), total organic carbon (TOC), bulk nitrogen isotopes, total organic nitrogen, carbon/nitrogen ratios, elemental X-ray fluorescence data, grain size, and presence of laminated or dysoxic, green intervals. Principal component analysis of these data captures key climatic intervals. The LGM was characterized by low productivity across the region. In the Bering Sea, deglaciation began around 18–17 ka, with increasing terrestrial sediment and TOC input. Marine productivity increased during the Bølling-Allerød when laminated sediments revealed dysoxic bottom waters where denitrification was extreme. The Younger Dryas manifested increased terrestrial input and decreased productivity, in contrast with the Pre-Boreal, when productivity markedly rebounded. The Pre-Boreal and Bølling-Allerød were similarly productive, but changes in the source of TOC and a $\delta^{13}C_{org}$ depletion suggest the influence of a gradually flooding Bering Shelf during the Pre-Boreal and Holocene.

1. Introduction

The Arctic and high northern latitudes have experienced the greatest impacts of climate change unfolding over the past 100 years (Intergovernmental Panel on Climate Change, 2013). This warming may be put into context by examining the records of changing climatic and oceanographic conditions during previous periods of warming. Following the LGM and prior to the Holocene, deglaciation occurred during a period of dramatic global climate change, which profoundly impacted the northern high latitudes. The North Pacific Ocean and Bering Sea thus provide an ideal natural laboratory to examine the expression of climatic and oceanographic change in high-latitude marine sediments.

Here we use sedimentologic, geochemical, and isotopic evidence to build upon previous studies of the Bering Sea (e.g., Brunelle et al., 2010; Caissie et al., 2010, 2016; Cook et al., 2005; Kuehn et al., 2014; Sancetta et al., 1985; Schlung et al., 2013), Gulf of Alaska (Addison et al., 2012; Barron et al., 2009; Davies et al., 2011), and North Pacific (Keigwin et al., 1992; Kohfeld & Chase, 2011; Lam et al., 2013). These studies focused on diatoms, radiolarians, foraminifera, alkenones, and stable isotopes as proxies for environmental change during the late Quaternary and Holocene. Many of these studies emphasized the timing and characteristics of deglacial, laminated sediments. Our millennial-scale, multiproxy study complements the growing body of North Pacific paleoclimate records by measuring organic carbon isotopes, total organic carbon (TOC), bulk nitrogen isotopes, total organic nitrogen, carbon/nitrogen ratios, elemental X-ray fluorescence (XRF) data, and grain size from sediment cores in the Bering Sea. We use bulk biogeochemical and isotopic data to estimate relative productivity, nutrient utilization, and sediment sourcing across the marine sector of Beringia, that is, the shallow marine shelves of the Bering, East Siberian, Chukchi, and Beaufort Seas.

Our findings describe millennial-scale changes in productivity and terrestrial input and offer a new suite of evidence to aid interpretations of the drivers of observed changes in the Bering Sea during the most recent period of rapid environmental change.
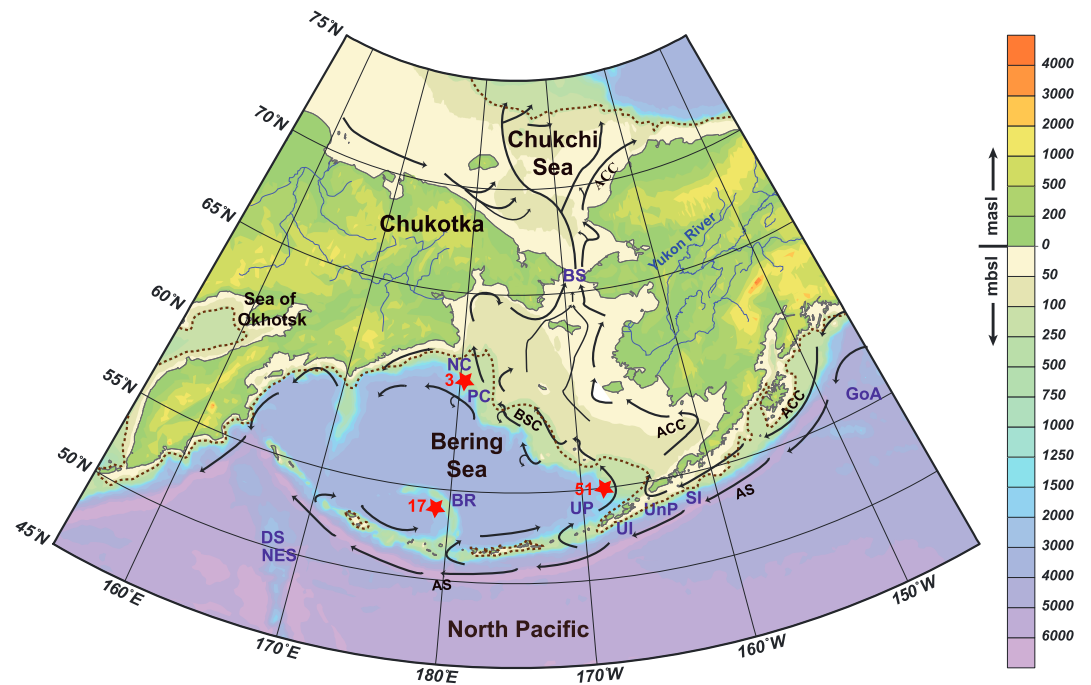
Figure 1. Bathymetric and topographic map of Beringia, the North Pacific Ocean, and the Bering and Chukchi Seas, with locations of cores (numbered red stars, Table 1). Currents denoted by black arrows: Alaska Coastal Current (ACC), Alaskan Stream (AS), and Bering Slope Current (BSC). The Bering Strait (BS), Bowers Ridge (BR), Detroit Seamount (DS), Gulf of Alaska (GoA), Navarin Canyon (NC), Northern Emperor Seamounts (NES), Pervenets Canyon (PC), Sanak Island (SI), Unalaska Island (UI), Unimak Pass (UnP), and Umnak Plateau (UP) are labeled in blue. The dashed line indicates the estimated shoreline during the LGM with sea level 120–125 mbp (Peltier & Fairbanks, 2006).

2. Background

2.1. Bering Sea

An extensive continental shelf (50–150 m deep) in the north and three deep basins reaching depths up to 4,000 m in the south characterize the Bering Sea (Figure 1). Shelf waters primarily flow north through the Bering Strait, which averages 50 m below present sea level (Schumacher & Stabeno, 1998). The Bering Sea is nutrient rich today (Cooper et al., 1997; Roach et al., 1995), particularly across the shelf and slope region where high nutrient waters of deep North Pacific origin are upwelled (Walsh et al., 1989). Three currents constrain cyclonic circulation around the deep basins, while the Bering Slope Current, known for high primary productivity (Hurst et al., 2010; Kinney et al., 2009), flows along the continental shelf break, defining the eastern edge of the gyre (Schumacher & Reed, 1992). The Alaska Coastal Current brings 0.23 sverdrupof Pacific water through Unimak Pass (<80 m deep), and up onto the shelf (Stabeno et al., 1999).

The Bering Sea is the largest and northernmost marginal sea in the North Pacific and is home to some of the highest primary productivity in the global ocean (Sambrotto et al., 1984; Springer et al., 1989, 1996). It serves as the connection between the Pacific and Arctic Oceans, and along with the shallow Chukchi, Beaufort, and East Siberian Seas, is the marine portion of Beringia. Beringia (Figure 1) was defined by Hopkins (1959) to include these shallow shelves as well as the terrestrial regions of eastern Russia and Alaska stretching from the Lena River to the Mackenzie River. The term Bering Land Bridge is commonly used with reference to largely the central region of Beringia, including those areas exposed during the LGM. Beringia and the Bering Sea are, currently and historically, climatically and biologically critical regions in their role as the connection between the Arctic and Pacific Oceans and in the migration of terrestrial species during low sea level stands (De Boer & Nof, 2004; Goosse et al., 1997; Hopkins, 1979, 1982; Hu et al., 2014; Hu & Meehl, 2005; Shaffer, 1994).

2.2. Recognition of Prevalent Laminated Sedimentation

Widespread deposition of laminations occurred in North Pacific sediments during the Bølling-Allerød (14.9–12.9 ka) and Pre-Boreal (~11.7–10.7 ka) (Mangerud et al., 1974; Van der Plicht et al., 2004) warm

Table 1
Cores Used in This Study

Location	Core	Depth (m)	Length (m)	Latitude/longitude	Previous work
Bering Slope	HLY0202-3JPC	1132	14.4	N60.12791/E180.55821	Cook et al. (2005)
Bowers Ridge	HLY0202-17JPC	2209	3.1	N53.93301/E178.69881	Cook et al. (2005) and Brunelle (2007, 2010)
Umnak Plateau	HLY0202-51JPC	1467	4.2	N54.55321/E191.33311	Caissie et al. (2010)

periods. The early Holocene was characterized globally by warmer temperatures (Meyer et al., 2017), and in the Bering Sea by increased productivity and laminated sediments (e.g., Kuehn et al., 2014). Laminations from these time periods are found along the northwest coast of Mexico (Ganeshram & Pedersen, 1998), Gulf of California (Barron et al., 2005; Keigwin, 2002; Sancetta, 1995), Santa Barbara Basin (Hendy & Kennett, 2003; Kennett & Ingram, 1995), California margin (Gardner et al., 1997; Mix et al., 1999), northwestern Pacific (Brunelle et al., 2010; Keigwin et al., 1992; Shibahara et al., 2007), Sea of Japan (Takahashi, 1998), and the Bering Sea (Brunelle et al., 2007; Caissie et al., 2010; Cook et al., 2005; Itaki et al., 2009; Khim et al., 2011; Kim et al., 2011; Kuehn et al., 2014; Okazaki et al., 2010; Schlung et al., 2013).

Laminated sediments are deposited under dysoxic to anoxic conditions (Behl & Kennett, 1996; Kennett & Ingram, 1995) with export productivity and ventilation controlling benthic oxygenation (Hendy & Pedersen, 2005). Laminated intervals in cores proximal to our Bering Sea sites have been attributed to changes in oxygen content of North Pacific Intermediate Water and increased export production, the combination of which fostered dysaerobic conditions, though much remains unknown about the relative importance of each forcing mechanism (Caissie et al., 2010; Cook et al., 2005; Davies et al., 2011; Kuehn et al., 2014; Schlung et al., 2013).

3. Methods

The cores used in this study were collected using a jumbo piston corer during two legs (HLY02-02 and HLY02-04) of the Arctic West Summer 2002 cruise of the United States Coast Guard Cutter Healy (Table 1). Throughout the text, we refer to the following five time periods. The Last Glacial Maximum is broadly defined from 27 to 18 ka. The Early Deglacial (ED) (18–15 ka), when rapid changes were taking place globally, includes the cold Heinrich Stadial 1 period in the North Atlantic and concurrent atmospheric CO_2 rise and Southern Hemisphere warming (Van der Plicht et al., 2004). The Bølling-Allerød warm phase is (14.9–12.9 ka) (Rasmussen et al., 2006). The Younger Dryas is traditionally defined as 12.9–11.7 ka (Carlson, 2013). We refer to the early Holocene as the Pre-Boreal (PB) (11.7–10.7 ka) throughout the text to distinguish this unique interval from the rest of the Holocene (<10.7 ka) (Mangerud et al., 1974; Van der Plicht et al., 2004).

3.1. Age Models

Cores 3JPC, 17JPC, and the section of 51JPC chosen for our study were previously ^{14}C-dated (Table 2), using *Neogloboquadrina pachyderma* (sinistral), a planktic foraminifera (Cook et al., 2005). 51JPC contains two tephra deposits that were treated as instantaneous events. The lower of these has been correlated to the T11 tephra from Sanak Island and dated to 14.6 ± 0.1 ka (Misarti et al., 2012).

A reservoir age of 800 years (ΔR 400) was chosen to be consistent with published studies of these cores (Brunelle et al., 2007, 2010; Caissie et al., 2010; Cook et al., 2005), other proximal cores with calculated reservoir ages that range between 730 and 1,100 years near 3JPC (Itaki et al., 2009; Kim et al., 2011; Kuehn et al., 2014; Schlung et al., 2013), and the marine calibration data sets (http://calib.qub.ac.uk/marine/) (McNeely et al., 2006). However, this reservoir correction has been previously estimated to range between 460 to 1,100 years for total modern reservoir corrections (Dumond & Griffin, 2002; Gorbarenko et al., 2005; Kuzmin et al., 2001). Both the Younger Dryas (YD) and the termination of the last glacial stage may have had pronounced impacts on thermohaline circulation (Keigwin et al., 1991; J. F. McManus et al., 2004) and related reservoir ages when old carbon, sequestered in the glacial deep oceans, was upwelled and released to the atmosphere (Sarnthein et al., 2007). Indeed, Kuehn et al. (2014) counted varves from a core near 3JPC and correlated them to events in the North Greenland Ice Core (NGRIP). They then took the difference between these independently determined ages and planktic foraminiferal ^{14}C ages to show that the

Table 2
Uncorrected Accelerator Mass Spectrometry ^{14}C Ages, and Corrected, Calibrated Ages Measured on N. pachyderma (s.) in 3, 17, and 51JPC (Cook et al., 2005)

Core	Depth (cm)	^{14}C yr ± 1σ	yr B.P. ±		Material dated
3JPC	140.5–142.5	10,050 ± 60	10,530	10,700 10,370	*N. pachyderma*
3JPC	352.5–353.5	10,850 ± 65	11,580	11,880 11,280	*N. pachyderma*
3JPC	600.5–601.5	12,400 ± 65	13,460	13,610 13,300	*N. pachyderma*
3JPC	839.5–840.5	13,300 ± 70	14,670	15,070 14,280	*N. pachyderma*
3JPC	906.5–909.5	13,350 ± 80	14,740	15,140 14,330	*N. pachyderma*
3JPC	1,427.5–1,428.5	18,100 ± 130	20,900	21,250 20,540	*N. pachyderma*
51JPC	134.5–135.5	10,600 ± 60	11,200	11,340 11,060	*N. pachyderma*
51JPC	177.5–178.5	12,500 ± 60	13,560	13,720 13,390	*N. pachyderma*
51JPC	214.5–242.5	14,050 ± 85	15,930	16,190 15,670	*N. pachyderma*
51JPC	479.5–480.5	18,200 ± 110	21,000	21,340 20,680	*N. pachyderma*
17JPC	155.5–156.5	10,000 ± 60	10,460	10,630 10,290	*N. pachyderma*
17JPC	185.5–186.5	12,550 ± 65	13,600	13,780 13,430	*N. pachyderma*
17JPC	215.5–216.5	13,400 ± 60	14,920	15,210 14,630	*N. pachyderma*
17JPC	383.5–384.5	25,200 ± 130	28,420	28,740 28,100	*N. pachyderma*

Note. Calibrations were performed with Clam 2.2 (Blaauw, 2010) using ΔR = 400 years, corresponding to an ~800 year reservoir correction.

reservoir age was older during the YD (910 years) than during the Bølling-Allerød (BA) (875 years) and PB (11.7–10.7 ka; 770 years). Although these ages are regionally consistent with previously estimated ages, there may have been regional or local changes in upper depth and middepth water ventilation during the deglaciation (Kuehn et al., 2014), leading to the wide range of estimates previously reported for the North Pacific.

All ^{14}C ages were calibrated using Clam 2.2 (Blaauw, 2010) and the Marine13 calibration curve (Reimer et al., 2013). Age-depth models were created with Clam 2.2 using linear interpolation for minimal investigator bias (Figure 2). The only exception was 51JPC, where the correlation was adjusted to best include the T11 date without causing an unrealistic shift in age. While the age of contemporaneous laminated units matches well with regional studies, we present our data with the caveat that reservoir age could have fluctuated by several hundred years.

3.2. Inorganic Geochemical Analysis

All archive-half sections of our cores were logged on both a Multi-Sensor Core Logger (MSCL, GEOTEK), and a high-resolution, XRF core scanner (ITRAX, COX Analytical Systems).

The MSCL obtained magnetic susceptibility, GRAPE bulk density (gamma ray attenuation porosity evaluator), and high-resolution images. Magnetic susceptibility was measured using a point sensor (MS3E, Bartington) with a field of influence ~1 cm in diameter. GRAPE bulk density was obtained using a cesium-137 gamma source, which emits a narrow beam of collimated gamma rays with energies at 0.662 MeV.

The ITRAX XRF core scanner provides high-resolution elemental composition (from Al to U) and X-radiograph images (Löwemark et al., 2008) (detailed description of the ITRAX: (Croudace et al., 2006)). ITRAX XRF analyses
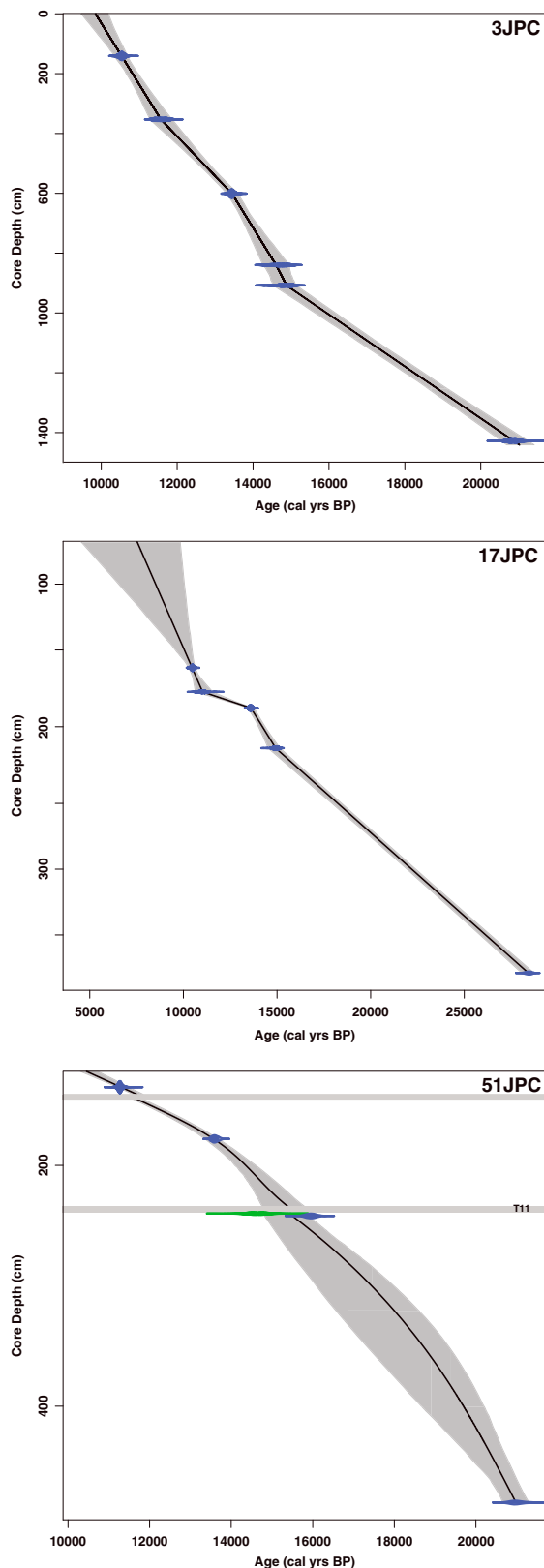
Figure 2. Age depth models for 3JPC, 17JPC, and 51JPC. The blue dots are ^{14}C ages, with 1σ error plotted (grey shading). Tephra (grey bars) were treated as instantaneous events in 51JPC with T11 date included (green dot).

were conducted with a Mo tube and 1,000 μm resolution. Without quantitative mineralogy (Eberl, 2004; Viscosi-Shirley et al., 2003), we do not interpret XRF elemental count data as quantitative, merely as a descriptor of relative changes in sediment composition.

3.3. Biogeochemical and Particle Size Analysis

The sediment cores were sampled for biogeochemical, isotopic, and grain size analysis using 1 cm diameter sediment plugs. 3JPC (129 cm kyr^{-1}) was sampled at 10 cm resolution in massive sections (Figure 3), with 5 cm resolution in both laminated intervals and the top meter of the core. 51JPC (31 cm kyr^{-1}) was sampled every 10 cm for grain size, and every 2 cm from 124 to 242 cm and 4 cm from 242 to 420 cm for $\delta^{13}C_{org}$ and %TOC. 17JPC (51 cm kyr^{-1}) was sampled every 10 cm.

3.3.1. Elemental Isotopic Analyses

Bulk biogeochemical properties ($\delta^{13}C_{org}$, $\delta^{15}N$, %TOC, %N$_{org}$, and C/N) were measured on an isotope ratio mass spectrometer with a Sercon GSL and Gilson gas autosampler prep unit (PDZ-Europa 20/20) (Figures 4 and 5). The isotopic data were measured by the Stable Isotope Research Unit of the Department of Crop and Soil Sciences at Oregon State University, Corvallis, OR. Samples were freeze-dried and ground to a fine powder before being treated with 1 M HCl to remove carbonate in samples used to measure $\delta^{13}C_{org}$ and %TOC (Ramnarine et al., 2011; Shultz & Calder, 1976). Replicate analyses indicated a standard deviation of 0.91 wt % for %TOC and 0.09‰ for $\delta^{13}C_{org}$. For $\delta^{15}N$, %N, and % total carbon, samples contained ~75 μg total N (55 mg sample). Replicate analyses indicated a standard deviation of 0.24‰ for $\delta^{15}N$ and 0.26 wt %N (Schubert & Calvert, 2001).

3.3.2. Carbon Isotope Mixing Models

The $\delta^{13}C_{org}$ of marine sediments can approximate relative proportions of terrigenous and marine organic carbon in sediment organic matter (OM) using a linear mixing model of terrigenous and marine OM (Hedges & Parker, 1976; Prahl et al., 1994; Shultz & Calder, 1976; Trefry et al., 2014), according to the following equation:

$$OC_{terr}(fraction) = \frac{\delta^{13}C_{sample} - \delta^{13}C_{mar}}{\delta^{13}C_{terr} - \delta^{13}C_{mar}}$$

This equation yields terrestrial organic carbon (OC$_{terr}$), which is then used to calculate marine organic carbon (OC$_{mar}$):

$$\%OC_{mar} = \%TOC_{sample} - (OC_{terr} \times \%TOC_{sample})$$

Depleted $\delta^{13}C_{org}$ values (−26 to −28‰) are typical of terrigenous OM using the C$_3$ pathway of photosynthesis (Ratnayake et al., 2006, 2005; Stein & Macdonald, 2004), as seen in the following regions: Mackenzie Beaufort terrigenous end-member: −26.5 to −27‰ (Naidu et al., 2000), Russian Rivers draining taiga/tundra: −26.5‰ (Lobbes et al., 2000), Yukon: −26 to −28‰ (Guo & Macdonald, 2006), and Gulf of Alaska: −26‰. Marine $\delta^{13}C_{org}$ is generally assumed to be > −25‰ (Grebmeier et al., 1988), with average marine phytoplankton values of −19 to −22‰ (Fontugne & Jouanneau, 1987; Meyers, 1994). We assigned −27‰ for the terrigenous OC end-member and −21‰ for the marine OM end-member for consistency with studies of Bering and Chukchi Seas (Naidu et al., 1993, 2000, 2004; Trefry et al., 2014; Walsh et al., 1989) and the Gulf of Alaska (Addison et al., 2012).
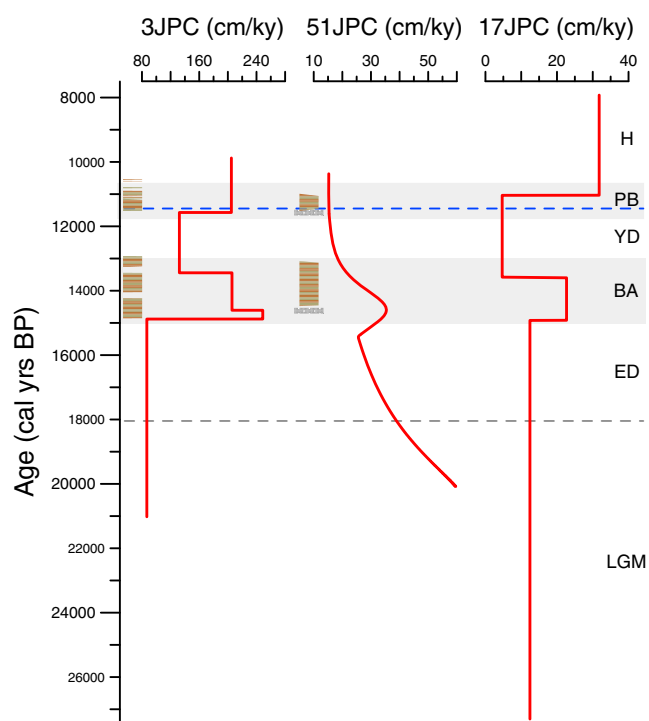
Figure 3. Sedimentation rate of each core as estimated by the age depth models of Figure 2. The blue dashed line marks the interval when relative sea level reached the sill depth of the Bering Strait (~50 m) (Waelbroeck et al., 2002), in agreement with Keigwin et al. (2006). Laminations are indicated by brown/green striped bars, and tephra as stippled light grey bars. The grey shading marks the BA and PB, with a grey dashed line delineating the relative ED/LGM transition. Climatic intervals: H = Holocene, PB = Preboreal, YD = Younger Dryas, ED = Early Deglacial, LGM = Last Glacial Maximum. Age-depth models were created with Clam 2.2 using linear interpolation except a smooth spline for 51JPC to best include the T11 date without causing an unrealistic shift in age.

3.3.3. C/N Ratios and %N_{org}

Arctic sediments often have high amounts of inorganic nitrogen bound to clay minerals (N_{bou}) (Stein & Macdonald, 2004), which can bias C/N ratios. To better represent source materials, we plotted TOC versus TN, where the y-intercept represents N_{bou} (Figure S1 in the supporting information) (Schubert & Calvert, 2001; Stein & Macdonald, 2004). We estimated organic nitrogen (N_{org}) using the following equation:

$$\%\textbf{\textit{N}}_{org} = \%\textbf{\textit{N}} - \%\textbf{\textit{N}}_{bou}$$
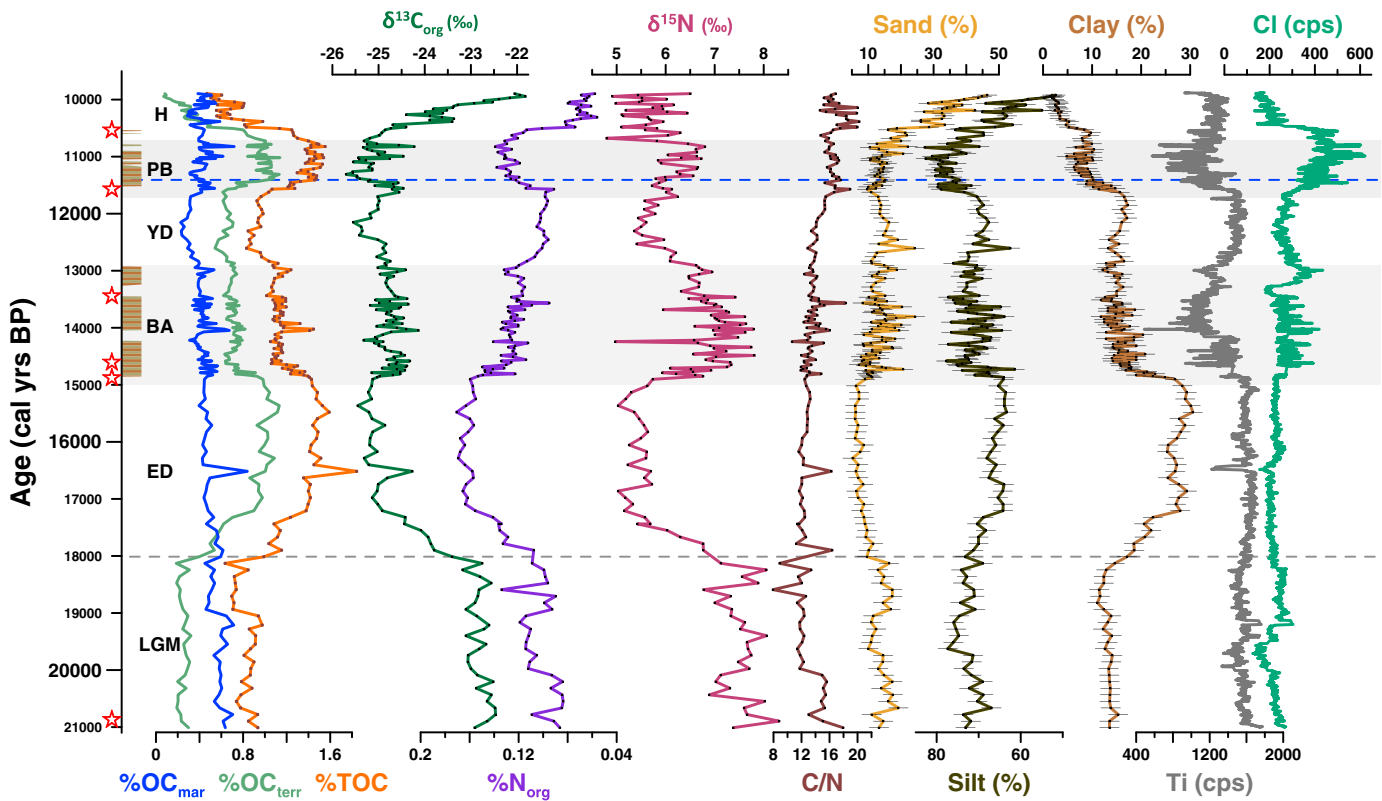
3.3.4. Grain Size Analysis

Grain size from 0.01 to 3,500 μm was measured on a laser diffraction particle size analyzer (Malvern Mastersizer 3000). Samples were not treated to remove carbonates, organics, or siliceous organisms (Aiello & Ravelo, 2012), and thus represent bulk grain size. We followed the Wentworth grain size chart (Wentworth, 1922) in defining our grain size intervals: clay <4 μm, silt 4–63 μm, and sand 63–3,500 μm (Aiello & Ravelo, 2012). Samples were run three times. The mean is reported along with 2σ error.

3.4. Principal Component Analysis

Principal component analysis (PCA) was completed for XRF, grain size, bulk biogeochemical, and isotopic data using MATLAB (MathWorks, 2014). Data were normalized (z-score) prior to PCA. PCA biplots of scores for both XRF data only and for a full suite of geochemical and sedimentologic parameters (hereafter referred to as full suite PCA) were produced to investigate shifts in sediment characteristics.

For full suite PCA, it was necessary to use the resolution of the most coarsely resolved data, the isotopes. Thus, the high-resolution data were down-sampled to 1 cm samples using a moving, centered, 11-point running average for the 1,000 μm XRF data, and a 3-point running average for 0.5 cm MSCL data, with averaged values representing a given centimeter selected to match isotopic sample locations.

4. Results

4.1. Western Bering Sea Shelf Slope, 3JPC

Jumbo Piston Core 3 (HLY02-02-3JPC) was taken between Navarin and Pervenets Canyons on the Bering Sea shelf slope (Cook et al., 2005), at 1,132 m water depth (Figure 1). At 14 m long, 3JPC contains the most expanded deglacial sequence in this study, with an average sediment accumulation rate of 185 cm kyr^{-1} (Figure 3). 3JPC contains four visibly laminated intervals, composed of triplets of dark and light olive lamina ranging in thicknesses from <1 to 2 mm. The first three laminated intervals occur during the BA (901–763 cm, 724–602 cm, and 574–533 cm) spanning 14.7–12.9 ka (Figure 3). The final interval was deposited during the Pre-Boreal from 11.5 to 10.8 ka (342–215 cm), though there are three minor laminae groups (2–5 cm) after 10.8 ka. Intervening massive intervals and the deepest 5.4 m of sediment are composed of homogeneous sticky dark olive-gray silty mud, characterized by slower sedimentation (87 cm kyr^{-1}).

During the LGM, $\delta^{13}C_{org}$ averaged −22.8‰ indicating predominantly marine TOC before a swift decline at 18 ka to −25‰ (Figure 4), during which time OC_{terr} surpassed OC_{mar}. The $\delta^{13}C_{org}$ remained depleted until ~10.7 ka when it increased to −21.8‰ coincident with the cessation of laminations and decrease in TOC, re-establishing OC_{mar} as the primary source of organic carbon.

The $\delta^{15}N$ values (average 7.5‰) and C/N ratios were high (average 15.3) during the early LGM, with C/N dropping to 12 before increasing during the early Holocene. A rapid decrease in $\delta^{15}N$ occurs around 18 ka (Figure 4) before rising again during the BA. The $\delta^{15}N$ fell below 5.5‰ during the YD, prior to increasing entering the Pre-Boreal (PB) and fluctuating around 5.5‰ during the early Holocene.

Figure 4. 3JPC %TOC, estimated %OC$_{terr}$ and %OC$_{mar}$, bulk $\delta^{13}C_{org}$, %N$_{org}$, bulk $\delta^{15}N$, C/N, grain size data, Ti, and Cl. Ti and Cl chosen to represent terrigenous sources and productivity, respectively. The blue dashed line marks the interval when relative sea level reached the sill depth of the Bering Strait (~50 m) (Lambeck et al., 2014), in agreement with Keigwin et al. (2006). Laminations are indicated by brown/green striped bars, and tephra as stippled light grey bars. The grey shading marks the BA and PB, with a grey dashed line delineating the relative ED/LGM transition. The red stars represent six ^{14}C dates, given in calendar years (Cook et al., 2005). The blue arrow is the window of Bering Strait flooding (Keigwin et al., 2006).

Median grain size averaged 14 μm from 21 to 10.8 ka, before increasing to 35 μm from 11 to 9.8 ka with greater sand and silt (Figure S2). Clay averaged 13% during the LGM, before peaking at 28% during the Early Deglacial (ED). Clay content rapidly decreased at the onset of the BA, and further fell at the YD/Holocene transition, reaching the lowest value of the record (<2%) by the core top.

During the laminated intervals in 3JPC, there is a decrease in Ti, Fe, K, and Rb and an increase in Cl, Br, and to a lesser extent Ca. In contrast, Ti, Fe, K, and Rb are highest during the LGM, ED, and YD (Figure S3). In the full-suite PCA analysis, the data are similarly influenced by both PC1 (31%) and PC2 (24%) (Figure 6). The ED samples plot closest to Fe, Ti, K, Rb, and clay, and the PB and BA show variability, but plot closest to %TOC, %N$_{org}$, silt, Cl, and Br. Sediment younger than 10.5 ka is a clear anomaly and plots closest to sand. In the XRF PCA (Figure S4), the YD plots at the origin, between the LGM/ED to the right (terrestrial) and the BA/Holocene populations to the left (productivity). The samples plot along PC1 from right to left with age in the XRF PCA, which explains 40% of the variability.

4.2. Southwest Bering Sea, Bowers Ridge, 17JPC

17JPC (HLY02–02-17JPC), the southern-most and deepest core (2,209 m water depth), was taken from Bowers Ridge (Cook et al., 2005) (Figure 1). Spanning nearly 20,000 years, 17JPC comprises the longest record of this study (27 to 8 ka), contained in only 3 m of massive diatomaceous olive green-grey silty mud with an average sedimentation rate of 20 cm kyr^{-1} (Figure 3). Green layers characterize the BA and PB, which are rich in OM, CaCO$_3$, and biogenic opal and correlate temporally with laminated intervals in 3JPC (Brunelle et al., 2007; Cook et al., 2005).

The $\delta^{13}C_{org}$ of 17JPC averages −22.2‰ with minimal variability outside of an enrichment and subsequent depletion during the BA (Figure 5); thus, OC$_{mar}$ comprises nearly all TOC preserved in 17JPC. TOC is low
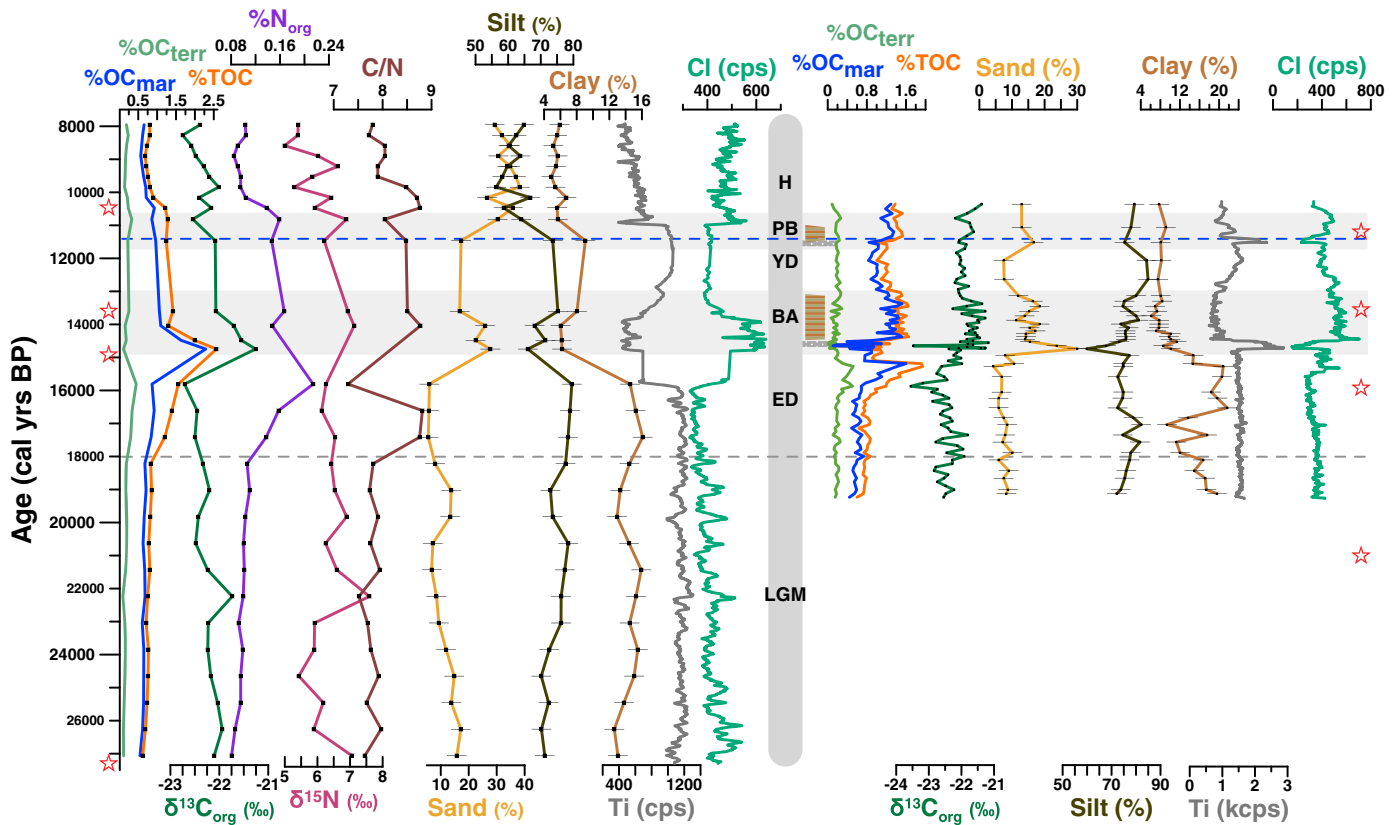
Figure 5. (left) 17JPC and (right) 51JPC: %TOC, estimated %OC$_{terr}$ and %OC$_{mar}$, bulk $\delta^{13}C_{org}$, %N$_{org}$, bulk $\delta^{15}N$, C/N, grain size data, Ti, and Cl. Ti and Cl chosen to represent terrigenous sources and productivity, respectively. The red stars are ^{14}C dates given in calendar years (Cook et al., 2005). The blue dashed line marks the interval when relative sea level reached the sill depth of the Bering Strait (~50 m) (Lambeck et al., 2014), in agreement with Keigwin et al. (2006). Laminations are indicated by brown/green striped bars, and tephra as stippled light grey bars. The grey shading marks the BA and PB, with a grey dashed line delineating the relative ED/LGM transition.

during the LGM (0.75%), increases during the ED and peaks at 2.5% during the BA. The $\delta^{15}N$ averages 6.3 ± 0.68‰ throughout the record, but due to low resolution, no trends can be confidently described (Figure 5). The %N$_{org}$ averages 0.13 ± 0.07% and is assumed to be equivalent to %N$_{org}$ in 17JPC because %N$_{bou}$ is near zero (0.01%; Figure S1) (Stein & Macdonald, 2004).

Ti, Mn, Fe, K, and Rb are abundant from 27 to 16 ka before a minimum during the BA, coincident with an increase in sand-size particles and median grain size, and then rebound during the YD (Figures 5, S2, and S5). After 11 ka, these elements decrease to counts comparable to those of the BA with abundant Sr, Ca, Br, and Cl and increased median grain size.

Full suite PCA (Figure 6) reveals that the LGM and ED plot proximal to terrigenous end-members, with the Holocene associated with sand, similar to 3JPC, and the BA plotted closer to productivity end-members. The data are primarily influenced by PC1 (54%), but PC2 explains a significant portion of the variance (17%). In the XRF PCA (Figure S4), the YD plots between the LGM/ED and the BA/Holocene populations. As with 3JPC, the samples plot along PC1 from right to left with age in the XRF PCA, which explains 72% of the variability.

4.3. Southeast Bering Sea, Umnak Plateau, 51JPC

51JPC (HLY02-02-51JPC) was taken from 1,467 m water depth on the Umnak Plateau in the southeast Bering Sea (Caissie et al., 2010; Cook et al., 2005), about 130 km northwest of Unalaska Island (Figure 1). Data were collected for this study from 120 to 420 cm covering 10.2 to 19.2 ka. 51JPC is composed of relatively homogenous diatomaceous dark olive-green clay and silt, punctuated by two tephra deposits that are each followed by a laminated interval (Figure 5). The first laminated interval occurs during the BA and the second
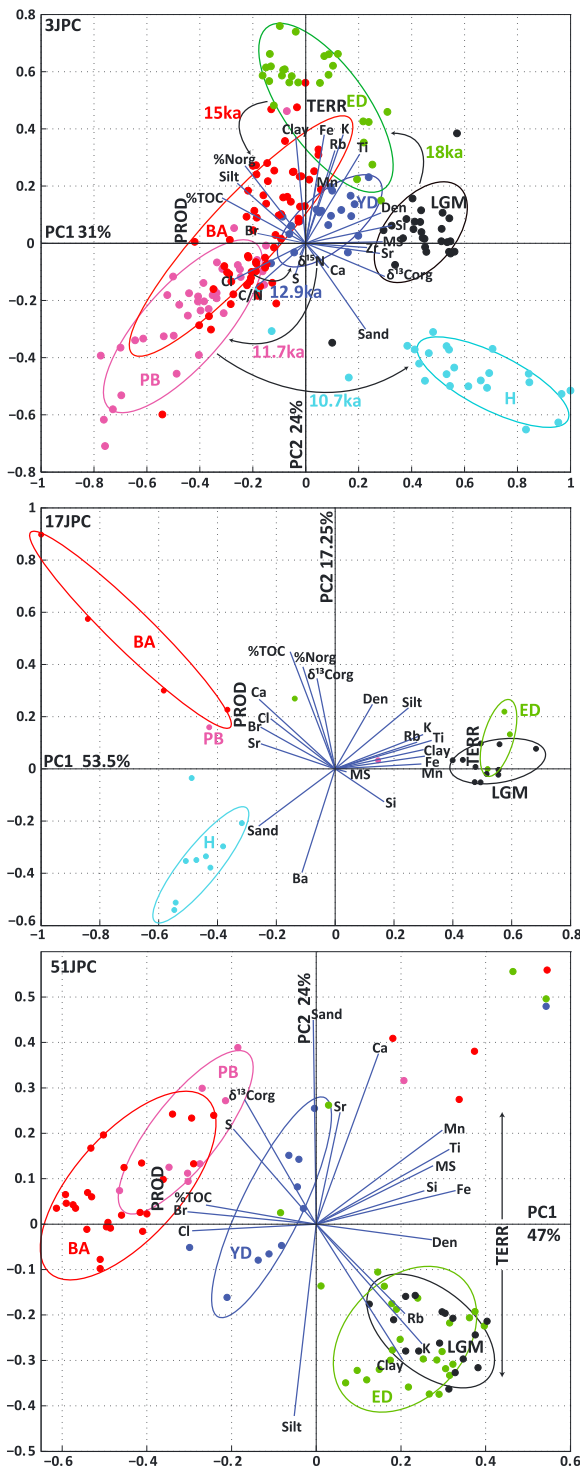
Figure 6. Full suite PCA biplots with populations color coded by age. PC1 and PC2 are principal components one and two, with percent variation explained. The blue lines are PC coefficients for each variable. TERR and PROD represent the area of terrestrial and productivity end-members, respectively (as defined in section 5.1). Climatic intervals are color coded as follows: Last Glacial Maximum (LGM) 27–18 ka, black; Early Deglacial (ED) 18–15 ka, green; Bølling-Allerød (BA) 14.9–12.9 ka, red; Younger Dryas (YD) 12.9–11.7 ka, blue; Preboreal (PB) 11.7–10.7 ka, and the Holocene (H) 10.7 ka to present, cyan.

in the PB. The laminations are composed of black to dark olive green-grey submillimeter-thick lamina. Sediment accumulation rate declines from 42 cm kyr^{-1} from the LGM until ~16 ka when the rate increases to 21 cm kyr^{-1} during the BA laminations before slowing to 15 cm kyr^{-1} into the Holocene (Figure 3).

OC_{mar} is the dominant component of TOC throughout the record, with $\delta^{13}C_{org}$ averaging −22.1‰, indicative of a marine signal (Figure 5). During the LGM and into the ED, values are already relatively enriched (−22.5‰), but increase more ~15.5 ka, with $\delta^{13}C_{org}$ steady at −21.8‰ from the BA into the Holocene. TOC is lowest during the LGM, peaks at the end of the ED, then drops at the start of the BA before flattening out to the end of the record. Clay was most abundant during the ED, and decreased at the onset of the BA with an increase in sand content, driving median grain size higher from the BA into the early Holocene (Figure S2).

Ti, Mn, Fe, K, and Rb counted highest during the LGM, ED, and YD, while decreasing during the BA and PB. With the tephra units removed, both the full suite and XRF PCA display the ED and LGM plotted together, near Rb, K, and clay (Figures 6 and S4). The BA has two populations, which is seen best in the XRF PCA (Figure S4), with the smaller population representing the samples with high terrigenous end-members, possibly due to fine tephra material contaminating the sediment above the actual tephra blocks, and the primary population plots with the productivity end-members. The YD is in the center of both PCA plots, and the Holocene is between the main BA and PB samples (Figures 6 and S4).

5. Discussion

5.1. Principal Component Analysis End-Member Selection

We identify Fe, Ti, K, and Rb as terrigenous end-members in our data. They are terrestrially derived products, common elements in mafic minerals, and are abundant in Alaska and Chukotka (Asahara et al., 2012; Beikman, 1994). For each core, these elements plot together in PCA (Figure 6). Clay plots near the terrigenous end-members for each core but was not selected since clay-sized grains originate from both terrestrial (e.g., siliciclastic grains) (Asahara et al., 2012; Nagashima et al., 2012) and marine sources (e.g., diatom fragments) (Aiello & Ravelo, 2012). Si and Mn both plot near terrigenous end-members but were not strongly correlated (Pearson's R values of 0.35 to 0.58) with the other terrigenous elements, which had R values of 0.68 to 0.88 in relation to each other. Si is the primary component of quartz grains, diatoms, and other siliceous microfossils and thus is both a component of terrigenous and biogenic sediments. The productivity end-members are %TOC, %N_{org}, Br, and Cl. TOC provides a first-order estimate of paleoproductivity (Stein, 1986) but can be influenced by terrestrial carbon input as well as OC accumulation rates, which are affected by oxygenation. Br and Cl are concentrated in sedimentary OM (Harvey, 1980; Price & Calvert, 1977), with Br strongly bonded to OM. Cl, associated with sea salt, is elevated in OM-rich sediment in our cores. There is evidence that Cl can be incorporated into marine organic matter when particulate algal material is used as a substrate for abiotic reactions (Leri et al., 2015), though we have no way of determining if this process is occurring in the Bering Sea. We do not propose that Cl

can be used as a proxy for productivity, rather we simply recognize its association with other productivity proxies. Likewise, XRF Br data have been directly related to TOC, but the relationship is weaker during intervals of high terrestrial carbon input (Ziegler et al., 2008). In certain cores, other variables appear to be associated with productivity, like Sr and Ca in 17JPC (Figure 6). As much as 40% of silt content variability can be explained by diatom abundance in the Bering Sea (Aiello & Ravelo, 2012), but terrigenous silt can also be transported (D. A. McManus et al., 1974), and generally plots between terrigenous and productivity end-members in full suite PCA biplots (Figure 6).

5.2. Last Glacial Maximum (27 to 18 ka)

Around 26 ka, the Bering Strait was closed (Hopkins, 1959). The Bering and Chukchi Seas were smaller than present day (Figure 1) due to the exposure of the continental shelves and sea level at 120 to 125 m below modern (Fairbanks, 1989; Peltier & Fairbanks, 2006). The cold climate of the LGM permitted extensive sea ice cover over the Bering Sea (Caissie et al., 2010; Katsuki & Takahashi, 2005; Sancetta et al., 1985). Reducing Alaskan Stream injection through Aleutian Passes would have limited the strength of the Bering Slope Current (Okazaki et al., 2005), isolated the southeastern Bering Sea, and supported sea ice growth (Overland & Pease, 1982). 51JPC may have been covered by sea ice nearly year-round as evidenced by high proportions of a diatom associated with multiyear ice, *Thalassiosira antarctica* resting spores, and epontic diatoms (Caissie et al., 2010).

Extensive sea ice cover could have limited wind forcing, weakening the strength and quantity of Bering Slope Current eddies, which drive active upwelling and associated high productivity (Clement et al., 2005). All sites had limited biological activity, indicated by low TOC (Figures 4 and 5) and lower sedimentation rates at 3JPC. Site 17JPC also records low productivity during the LGM (Figure 5) but was never covered by seasonal sea ice (Cook et al., 2005). The δ^{15}N values are high, similar to diatom-bound values from 17JPC (Brunelle et al., 2010). This is perhaps indicative of near complete nitrate utilization (which can occur when nitrate concentration is low) (Altabet & Francois, 1994; Sigman et al., 2001). However, when surface nitrate is entirely utilized, accumulating particulate organic matter shares the source nitrate's isotopic signature (Sigman et al., 2009), which is ~5–6‰ in the Bering Sea today (Lehmann et al., 2005). Therefore, the high values of δ^{15}N ($>$6‰) are suggestive of denitrification occurring after sediment deposition (Sigman et al., 2001). Inorganic nitrogen in clay minerals can influence bulk δ^{15}N (Schubert & Calvert, 2001); however, estimated inorganic nitrogen for both 17 and 3JPC (Figure S1), 8% and 20% respectively, suggests a possible minor effect in magnitude of δ^{15}N, but not of overall δ^{15}N trend.

17JPC is an open marine site, with no proximal major sources of terrigenous organic material from 27 to 8 ka. However, 3JPC and 51JPC were both less than ~200 km from land during the LGM (Peltier & Fairbanks, 2006). Nonetheless, there is a predominately marine $\delta^{13}C_{org}$ signal in all cores, which potentially supports either subice productivity with minimal sea ice melt or low open water productivity.

PCA of geochemical and isotopic data from 3JPC reveals that the LGM samples plot separately from other age-grouped samples (Figure 6), far from both the productivity and terrigenous end-members, suggestive of low productivity and a marine carbon source. However, the LGM plots near the terrigenous end-members in PCA plots for both 51JPC and 17JPC (Figures 6 and S4). High XRF counts of Ti, Fe, K, and Rb during the LGM support increased terrestrial inputs, as do high clay percentages at all sites. This terrestrial input may have resulted from riverine erosion of land, glacial erosion from the Aleutian Islands, and northeast Chukotka (Gualtieri et al., 2000; Mann & Hamilton, 1995), or wind-blown sediments (Lam et al., 2013; Otosaka et al., 2004). Riverine transport is most likely because although loess deposition south of 17JPC at GGC-37 on the Detroit Seamount was highest during the LGM (Lam et al., 2013), terrestrial organic matter in the BOW-8a core from Bowers Ridge was predominantly from the high-latitude Bering Sea catchment via riverine input, with only minor contributions from westerly winds (Ratnayake et al., 2005, 2006). Additionally, the relative dearth of fine clay (4% fine clay ($<$2 μm) versus 14% total clay) suggests that eolian input is unlikely.

5.3. Early Deglaciation (ED, 18 to 15 ka)
5.3.1. Increased Terrestrial Influx

Four main lines of evidence support increased terrestrial input to the Bering Sea during the ED: $\delta^{13}C_{org}$ depletion, increased OC_{terr}, high counts of terrigenous elements, and all sites plotting near the terrigenous end-members in PCA biplots (Figure 6).

In 3JPC, the relative $\delta^{13}C_{org}$ depletion and TOC increase begin ~18 ka (Figure 4) signaling the initiation of deglaciation. In 51JPC and 17JPC, the most depleted $\delta^{13}C_{org}$ values occur slightly later during the ED. Organic matter in 51JPC and 17JPC remains predominately marine throughout the record, but OC_{terr} increases slightly during the ED (Figure 5). At 3JPC, OC_{terr} becomes dominant at 17.5 ka (Figure 4).

Peaks in clay content in all three sites during the ED are suggestive of coastal erosion and inundation, supplemented by dust storms similar to those that transport micronutrient-rich loess to the Gulf of Alaska (Crusius et al., 2011).

5.3.2. Nutrient Utilization During the Early Deglaciation

Changes in $\delta^{15}N$, $\delta^{13}C$, TOC, N_{org}, and grain size in the Bering Sea are apparently synchronous with Southern Hemisphere warming and the Heinrich Stadial 1 of the North Atlantic. Early deglacial $\delta^{15}N$ depletion concurrent with continued low primary productivity was seen across the North Pacific, in the Okhotsk Sea (Brunelle et al., 2010), and in the southern Bering Sea, including in 17JPC (Brunelle et al., 2010; Kohfeld & Chase, 2011; Nakatsuka et al., 1995). Our analyses of 17JPC $\delta^{15}N$ and TOC show a muted version of this pattern, likely due to the low resolution of our samples. Similarly, TOC values at 51JPC remain low during the ED, not peaking until 15 ka. Diatom analysis at 51JPC supports this low productivity during the ED (Caissie et al., 2010). Ice cover began to decrease during the early deglacial in parts of the Bering Sea, and the first occurrence of alkenones was dated to 16.7 ka in the southeast Bering Sea (Caissie et al., 2010). Despite declining sea ice cover and a slight increase in biogenic fluxes, the increase in productivity during this period was small (Kohfeld & Chase, 2011). This pattern is explained by an initial breakdown in stratification that could allow for an increase in surface nitrate coupled with light limitation (Brunelle et al., 2010). However, at the shelf-slope break, TOC increases concurrently with the $\delta^{15}N$ depletion in 3JPC. This is likely because more terrestrial OM was added to the Bering Sea from the shelf as sea level rose, but this increase in organic matter did not reach the southern Bering Sea (Figure 4), nor was it derived from increased marine productivity.

5.4. Bølling-Allerød (14.9 to 12.9 ka)

At the onset of the Bølling-Allerød an abrupt freshening/warming is recorded in planktonic foraminiferal $\delta^{18}O$ on the Bering shelf-slope (Cook et al., 2005), on the Umnak Plateau (Caissie et al., 2010), and in the Gulf of Alaska (Davies et al., 2011). This interval featured rapid Northern Hemisphere warming (Broecker, 1998), sea surface temperatures increasing to ~11°C at Bowers Ridge (Schlung et al., 2013), and Meltwater Pulse 1a (MWP 1a) (Weaver, 2003). MWP 1a increased eustatic sea level by 20 m over ~500 years (14.4 to 13.8 ka) and was likely derived primarily from Laurentia (Tarasov & Peltier, 2005).

Increased productivity marked the BA in many parts of the Bering Sea (Brunelle et al., 2010; Caissie et al., 2010; Cook et al., 2005; Gorbarenko, 1996; Kuehn et al., 2014; Riethdorf et al., 2013; Schlung et al., 2013). It is sometimes explained as a result of declining sea ice coverage or nutrient input from flooding of the shelf. Alternatively, freshening from MWP 1a relieved light limitation by shallowing the depth of the mixed layer (Lam et al., 2013) and fostering elevated productivity. This light limiting effect is predicted by the critical depth theory (Sverdrup, 1953), which is valid in the western North Pacific (Obata et al., 1996).

Multiple lines of evidence are present for increased productivity at 3JPC, 17JPC, and 51JPC including deposition of laminated or green intervals. The BA is aligned with productivity end-members in our PCA biplots in all three Bering Sea cores (Figure 6). XRF data support higher productivity and a weaker terrigenous signal with decreases in Ti, Fe, and K and increases in Cl and Br (Figures 4, 5, S3, S5, and S6). TOC peaks at the start of the BA on Bowers Ridge. The highest sustained TOC values occur during this time on the Umnak Plateau, but at the slope site, TOC decreased suggesting a relationship between sea level and primary productivity at this site. As the Bering Land Bridge was inundated, the erodible surface area was reduced and the distance to land increased. This decreased the supply of OC_{terr} at 3JPC; however, the supply of OC_{mar} remained relatively stable (Figure 4).

At both 17JPC and 3JPC $\delta^{15}N$ values are enriched during the BA, although there are only two samples from 17JPC. Brunelle et al. (2007) also found enriched values at 17JPC, as did Schlung et al. (2013) at U1340 on Bowers Ridge and Nakatsuka et al. (1995) in the Aleutian Basin. Enrichment is generally explained by increased nitrate utilization and/or the intensification of denitrification in the Bering Sea (Brunelle et al., 2007, 2010; Schlung et al., 2013). If nitrate concentrations remained stable between the ED and BA, but light limitation was reduced, the resulting higher primary productivity would have utilized more available nitrate.

However, changes in utilization typically affect both $\delta^{15}N$ and $\delta^{13}C_{org}$ of dissolved inorganic carbon, as seen for 3JPC, where $\delta^{13}C_{org}$ follows $\delta^{15}N$ in the LGM and ED. In the BA, $\delta^{13}C_{org}$ only show an ~0.5‰ enrichment, which is insufficient for an entirely utilization-driven $\delta^{15}N$ enrichment. In addition, $\delta^{15}N$ nearly reaches 8‰. This suggests that the $\delta^{15}N$ enrichment was caused by water column denitrification (Sigman et al., 2009). The source nitrate may have been influenced by change to the character of intermediate water (Crusius et al., 2004), but laminated intervals during the BA in both 3JPC and U1340, as well as a green interval in 17JPC, are indicative of poor oxygenation capable of fostering local water column denitrification. Our records provide further evidence of widespread denitrification around the North Pacific during the BA.

During the BA laminated section, there are two bioturbated gaps that last ~200 years each, the first beginning at ~14.2 ka and the second at ~13.5 ka. These bioturbated intervals may represent the Older Dryas period, and Inter-Allerød Cold Period (Benson et al., 1997; Lehman & Keigwin, 1992), and perhaps mark a slight decrease in productivity, rendering oxygen utilization incomplete at depth, and/or better intermediate water ventilation (Mikolajewicz et al., 1997). This remarkable correspondence has been used to hypothesize that there is a teleconnection between Greenland and the Bering Sea (Kuehn et al., 2014) and the temporal correspondence of our bioturbated core intervals to NGRIP cold periods suggests that a large-scale change in climate was felt synchronously in Greenland and across the Bering Sea. The correspondence between 3JPC laminae deposition and the dating of the BA and YD in NGRIP (Rasmussen et al., 2006), and with other well-dated, regional cores with laminae (Behl & Kennett, 1996; Davies et al., 2011), is evidence that our age depth model is robust during this period.

5.5. Decreased Younger Dryas (12.9 to 11.7 ka) Productivity

The Beringian landmass was shrinking in extent but was likely still contiguous at the onset of the Younger Dryas (YD). Sea level rise was slowing (Bard, Hamelin, & Delanghe-Sabatier, 2010) as alpine glaciers advanced in Alaska (Briner et al., 2002). After declining during the BA, sea ice rebounded during the YD over the Umnak Plateau in the Bering Sea as productivity declined (Caissie et al., 2010; Cook et al., 2005). Such rapid climatic changes had a pronounced effect on marine species assemblages and regional productivity (Barron et al., 2009; Cook et al., 2005; Gorbarenko et al., 2005).

The YD marked a hiatus in laminae deposition in 3JPC and 51JPC. This hiatus is attributed to an increase in oxygenation due to changes in North Pacific Intermediate Water ventilation (Kennett & Ingram, 1995; Max et al., 2014; Okazaki et al., 2014; Zheng et al., 2000), primary productivity (Crusius et al., 2004; Mix et al., 1999; Schlung et al., 2013), or a combination of both (Gorbarenko et al., 2014; Hendy & Pedersen, 2005; Ishizaki et al., 2009; Kim et al., 2011). The massive sediment character of the YD is marked by decreased productivity in all three Bering Sea cores with decreased sedimentation rate, TOC, N_{org}, and depletion of $\delta^{13}C_{org}$.

At Bowers Ridge, the YD is identified as an 11 cm interval in U1340 (Schlung et al., 2013), and a 6 cm section in 17JPC that coincided with a collapse in biogenic Ba, $CaCO_3$, and opal (Brunelle et al., 2007). Low sedimentation rates were common during the YD (Figure 3) as seen on Bowers Ridge (10 cm kyr^{-1} (Schlung et al., 2013), 4–5 cm kyr^{-1} 17JPC), in the Gulf of Alaska (9 cm kyr^{-1}) (Davies et al., 2011), and on the Umnak Plateau (15 cm kyr^{-1}, 51JPC).

At 3JPC, $\delta^{13}C_{org}$ remained depleted during the YD with a slight decrease, consistent with reduced marine carbon flux resulting from decreased productivity. Low productivity is also evident from reduced TOC at both the slope site and the Umnak Plateau. At 3JPC, $\delta^{15}N$ depletion (Figure 4) is likely mostly indicative of reduced denitrification in oxygenated sediments (Brunelle et al., 2010; Schlung et al., 2013), as laminations were absent during the YD.

Terrigenous elements are abundant in all three cores during the YD, with an increase beginning ~13.5 ka. PCA biplots for the Bering Sea cores display the YD near the center, demonstrating that the YD was not as productive as the BA or PB and had less terrestrial input than the ED due to the Beringian shoreline becoming more distal, but this time period was not as biologically dormant as the LGM. Decreased productivity during the YD was seen across the Bering Sea and North Pacific (Gorbarenko, 1996; Nakatsuka et al., 1995; Riethdorf et al., 2013; Schlung et al., 2013). For 17JPC this can only be seen for the XRF PCA (Figure S4), as the isotopic data are too coarse to capture the YD.

5.6. Pre-Boreal (Early Holocene, 11.7 ka to 10.7 ka) and Holocene

The PB marked the end of the YD and contains the second major laminated interval seen in 51JPC and 3JPC, and across the North Pacific (e.g., Behl & Kennett, 1996). These laminations coincide with an abrupt freshening/warming event recorded in planktonic foraminifer $\delta^{18}O$ and alkenone-derived $U^{K'}_{37}$ SSTs at 11.65 ka (Caissie et al., 2010; Cook et al., 2005) and are indicative of an ameliorating climate with elevated productivity (Crusius et al., 2004; Davies et al., 2011; Khim et al., 2011; Schlung et al., 2013). Increased organic matter (Figures 4 and 5), the high prevalence of productivity indicators in PCA plots (Figure 6), and the presence of laminated intervals in 3JPC and 51JPC all support high productivity at this time.

Diatom evidence indicates rapid and significant influence of the Alaskan Stream as Unimak Pass was flooded (Caissie et al., 2010) at the onset of the PB. This ended the isolation of the southeastern Bering Sea and led to the disappearance of sea ice at Umnak Plateau (Caissie et al., 2010), increasing productivity by relieving light limitation (Lam et al., 2013). The strength of the Bering Slope Current is driven by the Alaskan Stream, so it likely increased at this time (Kim et al. (2011). This would have led to an increase in upwelling nutrients near Umnak Plateau and along the shelf-slope break (Johnson et al., 2004; Kinder et al., 1975; Okkonen et al., 2004) fostering high primary productivity. Today, these upwelled nitrate-rich waters become Bering Shelf Waters and carry nutrients into the Chukchi Sea below the sea ice during winter (Cooper et al., 1997; Tremblay et al., 2015). Prior to complete inundation of Bering Strait, however, we assume that these nutrients would stay trapped in the Bering Sea contributing to further high productivity here.

Global eustatic sea level, which was rising 12–15 m ka^{-1} at this time, did not reach the sill height of the Bering Strait (−50 m) until around 11.7 or 11.4 ka (Lambeck et al., 2014). Keigwin et al. (2006) posit that Bering Strait was breached as early as 12 ka, suggesting that relative sea level in Beringia reached the sill height slightly earlier due to minor isostatic rebound (Keigwin et al., 2006). However, the effect of opening the Bering Strait gateway was likely not instantaneous, but steadily increasing with ongoing sea level rise as a consequence of the inferred topography of the continental shelves at the time. Indeed, earlier researchers, argued that Bering Strait was not flooded until 11 ka and that there may have been an embayment just north of Bering Strait in what is now the Chukchi Sea (Elias et al., 1996). New work supports full inundation of Bering Strait not occurring until 11 ka, coincident with MWP 1b (Jakobsson et al., 2017).

If we assume that the flooding of the Bering Strait would have changed surface ocean circulation, allowing full connectivity between the Pacific and the Arctic Oceans via the Bering Slope Current and Bering Shelf Waters, then we would expect to see evidence of this inundation in southern Bering Sea cores. However, there is no change in any proxy between 12 and 11.7 ka and it is difficult to find a mechanism for why flooding of the Bering Land Bridge would drive high productivity at 11.7 ka, the start of the PB. Instead, we propose that the high productivity across the southern Bering Sea coupled with the dominance of OC_{terr} at the slope site (3JPC) provides evidence that Bering Land Bridge was not fully inundated until around 10.7 ka when productivity decreased, laminations terminated, and 3JPC became dominated by OC_{mar} again. This is very similar to the evidence from Herald Canyon in the Chukchi Sea, where the environment changes from a near-shore location with high terrigenous input, to an open marine continental shelf as Bering Strait flooded (Jakobsson et al., 2017).

Similar to the BA (Cook et al., 2005; Schlung et al., 2013), the PB productivity spike caused a return to suboxic conditions and thus an increase in local denitrification spurring a ~1.5‰ $\delta^{15}N$ enrichment. Following the PB laminations and productivity peak, $\delta^{15}N$ returns to YD levels.

PCA illustrates that 3JPC plots with sand for samples from the core top dated to the Holocene. A modern core (MC25) taken only 6 km from 3JPC had a large sand content despite its distance from the coast (Nagashima et al., 2012). The sediment in this interval in the nearby International Ocean Discovery Program site, U1345, is composed of quartz, feldspar, rock fragments, and some volcaniclastic material (Expedition 323 Scientists, 2011). The abundance of sand may be a result of reworked relict deposits from rivers that cut across the subaerial shelf during the last deglaciation (Nagashima et al., 2012). Alternatively, the Bering Slope Current could have increased in strength with the increased northward flow, preventing deposition of fine grain terrestrial material, making the top of core 3JPC a contourite (Hans Nelson et al., 1993).

6. Conclusions

Deglaciation following the LGM was characterized by significant climatic changes, which had a profound effect on the sediment delivery, circulation, and productivity of the Bering Sea. Sedimentological, geochemical, and isotopic evidence presented here from three Bering Sea cores offer insight into the timing and details of this climatically dynamic period when central Beringia flooded and the North Pacific and Arctic Oceans were reconnected via the submergence of the Bering Strait.

All cores record millennial-scale climate events since the LGM with the ED and YD associated with low productivity, enhanced sea ice in some cases, and decreased nitrate utilization, while the BA and PB are associated with laminated intervals or dysoxic sediments, higher primary productivity, decreased sea ice, and high denitrification.

The slope site, 3JPC, is most influenced by changing sea level due to its proximity the Bering Sea Shelf. Marine OM dominates at 3JPC only during the earliest Holocene and LGM. Terrigenous material dominates as sea level rises from the ED through the PB. Farther south, despite several intervals when terrigenous input rises, marine organic matter comprises the majority of OM at the Umnak Plateau and Bowers Ridge throughout the record.

The predominately marine $\delta^{13}C_{org}$ signal in 51JPC during the LGM seems contradictory to evidence of extensive sea ice over the Umnak Plateau, but may reflect subice productivity with minimal sea ice melt and associated export of terrigenous OM. Elemental abundances and PCA suggest high terrestrial input at Bowers Ridge (17JPC) during the LGM, but the relative dearth of fine clay suggests that the vast continental shelves and proximal land, rather than eolian deposition, were the primary sources of terrigenous input.

Deglaciation began in earnest around 18–17 ka, marked by depleted $\delta^{13}C_{org}$ indicating increasing terrestrial input and TOC. Productivity increased during the BA across the Bering Sea as illustrated by PCA. Previously hypothesized North Pacific denitrification related to dysoxia during the BA and PB is supported by an increase in bulk $\delta^{15}N$ in 3JPC during the laminated intervals. The sum of these data provides further evidence of large regional changes in productivity and water column ventilation through the deglaciation (Kao et al., 2008; Max et al., 2014). The presence of laminations and minimal $\delta^{13}C_{org}$ change, also support local water column denitrification.

Decreased sedimentation rate, TOC, N_{org}, $\delta^{13}C_{org}$ depletion, and a cessation of laminations characterized the YD, marking it as a period of increased terrestrial input and decreased productivity.

In the early Holocene, or Pre-Boreal, productivity markedly rebounded and conditions appear to have closely resembled those of the BA. While both the BA and PB were periods of elevated productivity, the PB was influenced by the effects of rising sea level. A strengthened Bering Slope Current would have carried deep Pacific nutrients up onto the narrow Bering Shelf driving primary productivity. It is not until the Bering Land Bridge is fully submerged, that these nutrients are seasonally carried farther north, productivity decreases, and dysoxia ceases in the Bering Sea. At this point also, the source of OC switches from terrigenous to marine at 3JPC. Depleted $\delta^{13}C_{org}$, a rapid TOC increase, and N_{org} decrease illustrate that the Bering Sea is influenced more by marine than terrigenous organic matter. The sandy core-top at 3JPC and transition from terrestrial to productivity end-members in the 17JPC illustrate the effect of the Bering Strait gateway on Bering Sea circulation. The opening of this gateway was not instantaneous, but progressive and amplified by continuing sea level rise.

The changes preserved in these three cores over the past 30 ka capture changes in productivity, nutrient delivery/utilization, sediment deposition, and circulation across the Bering Sea resulting from rapid climatic changes, the flooding of Beringia, and the re-opening of the Bering Strait.

References

Addison, J. A., Finney, B. P., Dean, W. E., Davies, M. H., Mix, A. C., Stoner, J. S., & Jaeger, J. M. (2012). Productivity and sedimentary $\delta^{15}N$ variability for the last 17,000 years along the northern Gulf of Alaska continental slope: Past Gulf of Alaska Productivity. *Paleoceanography*, *27*, PA1206. https://doi.org/10.1029/2011PA002161

Aiello, I. W., & Ravelo, A. C. (2012). Evolution of marine sedimentation in the Bering Sea since the Pliocene. *Geosphere*, *8*(6), 1231–1253.

Altabet, M. A., & Francois, R. (1994). Sedimentary nitrogen isotopic ratio as a recorder for surface ocean nitrate utilization. *Global Biogeochemical Cycles*, *8*(1), 103–116. https://doi.org/10.1029/93GB03396

Asahara, Y., Takeuchi, F., Nagashima, K., Harada, N., Yamamoto, K., Oguri, K., & Tadai, O. (2012). Provenance of terrigenous detritus of the surface sediments in the Bering and Chukchi Seas as derived from Sr and Nd isotopes: Implications for recent climate change in the Arctic regions. *Deep Sea Research Part II: Topical Studies in Oceanography*, *61–64*, 155–171. https://doi.org/10.1016/j.dsr2.2011.12.004

Bard, E., Hamelin, B., & Delanghe-Sabatier, D. (2010). Deglacial meltwater pulse 1B and Younger Dryas sea levels revisited with boreholes at Tahiti. *Science*, *327*, 1235–1237. https://doi.org/10.1126/science.1180557

Barron, J. A., Bukry, D., & Dean, W. E. (2005). Paleoceanographic history of the Guaymas Basin, Gulf of California, during the past 15,000 years based on diatoms, silicoflagellates, and biogenic sediments. *Marine Micropaleontology*, *56*, 81–102. https://doi.org/10.1016/j.marmicro.2005.04.001

Barron, J. A., Bukry, D., Dean, W. E., Addison, J. A., & Finney, B. (2009). Paleoceanography of the Gulf of Alaska during the past 15,000 years: Results from diatoms, silicoflagellates, and geochemistry. *Marine Micropaleontology*, *72*, 176–195. https://doi.org/10.1016/j.marmicro.2009.04.006

Behl, R. J., & Kennett, J. P. (1996). Brief interstadial events in the Santa Barbara basin, NE Pacific, during the past 60 kyr. *Nature*, *379*, 243–246.

Beikman, H. M. (1994). In G. Plafker & H. C. Berg (Eds.), *Geologic Map of Alaska*. Washington, DC: The Geology of Alaska: Geological Society of America.

Benson, L., Burdett, J., Lund, S., Kashgarian, M., & Mensing, S. (1997). Nearly synchronous climate change in the Northern Hemisphere during the last glacial termination. *Nature*, *388*(6639), 263–265.

Blaauw, M. (2010). Methods and code for "classical" age-modelling of radiocarbon sequences. *Quaternary Geochronology*, *5*(5), 512–518. https://doi.org/10.1016/j.quageo.2010.01.002

Briner, J. P., Kaufman, D. S., Werner, A., Caffee, M., Levy, L., Manley, W. F., … Finkel, R. C. (2002). Glacier readvance during the late glacial (Younger Dryas?) in the Ahklun Mountains, southwestern Alaska. *Geology*, *30*(8), 679. https://doi.org/10.1130/0091-7613(2002)030%C2%A0%3C%2%A00679:GRDTLG%3E2.0.CO;2

Broecker, W. S. (1998). Paleocean circulation during the last deglaciation: a bipolar seesaw? *Paleoceanography*, *13*(2), 119–121. https://doi.org/10.1029/97PA03707

Brunelle, B. G., Sigman, D. M., Cook, M. S., Keigwin, L. D., Haug, G. H., Plessen, B., … Jaccard, S. L. (2007). Evidence from diatom-bound nitrogen isotopes for subarctic Pacific stratification during the last ice age and a link to North Pacific denitrification changes. *Paleoceanography*, *22*, PA1215. https://doi.org/10.1029/2005PA001205

Brunelle, B. G., Sigman, D. M., Jaccard, S. L., Keigwin, L. D., Plessen, B., Schettler, G., … Haug, G. H. (2010). Glacial/interglacial changes in nutrient supply and stratification in the western subarctic North Pacific since the penultimate glacial maximum. *Quaternary Science Reviews*, *29*, 2579–2590. https://doi.org/10.1016/j.quascirev.2010.03.010

Caissie, B. E., Brigham-Grette, J., Lawrence, K. T., Herbert, T. D., & Cook, M. S. (2010). Last Glacial Maximum to Holocene sea surface conditions at Umnak Plateau, Bering Sea, as inferred from diatom, alkenone, and stable isotope records. *Paleoceanography*, *25*, PA1206. https://doi.org/10.1029/2008PA001671

Caissie, B. E., Brigham-Grette, J., Cook, M. S., & Colmenero-Hidalgo, E. (2016). Bering Sea surface water conditions during Marine Isotope Stages 12 to 10 at Navarin Canyon (IODP Site U1345). *Climate of the Past*, *12*(9), 1739–1763. https://doi.org/10.5194/cp-12-1739-2016

Carlson, A. E. (2013). The younger Dryas climate event. In S. A. Elias (Ed.), *The Encyclopedia of Quaternary Science* (Vol. 3, pp. 126–134). Amsterdam: Elsevier.

Clement, J. L., Maslowski, W., Cooper, L. W., Grebmeier, J. M., & Walczowski, W. (2005). Ocean circulation and exchanges through the northern Bering Sea 1979–2001 model results. *Deep Sea Research Part II: Topical Studies in Oceanography*, *52*, 3509–3540. https://doi.org/10.1016/j.dsr2.2005.09.010

Cook, M. S., Keigwin, L. D., & Sancetta, C. A. (2005). The deglacial history of surface and intermediate water of the Bering Sea. *Deep Sea Research Part II: Topical Studies in Oceanography*, *52*, 2163–2173. https://doi.org/10.1016/j.dsr2.2005.07.004

Cooper, L. W., Whitledge, T. E., Grebmeier, J. M., & Weingartner, T. (1997). The nutrient, salinity, and stable oxygen isotope composition of Bering and Chukchi Seas waters in and near the Bering Strait. *Journal of Geophysical Research*, *102*(C6), 12,563–12,573. https://doi.org/10.1029/97JC00015

Croudace, I. W., Rindby, A., & Rothwell, R. G. (2006). ITRAX: Description and evaluation of a new multi-function X-ray core scanner. *Special Publication-Geological Society of London*, *267*, 51.

Crusius, J., Pedersen, T. F., Kienast, S., Keigwin, L., & Labeyrie, L. (2004). Influence of northwest Pacific productivity on North Pacific Intermediate Water oxygen concentrations during the Bølling-Ållerød interval (14.7–12.9 ka). *Geology*, *32*, 633. https://doi.org/10.1130/G20508.1

Crusius, J., Schroth, A. W., Gassó, S., Moy, C. M., Levy, R. C., & Gatica, M. (2011). Glacial flour dust storms in the Gulf of Alaska: Hydrologic and meteorological controls and their importance as a source of bioavailable iron. *Geophysical Research Letters*, *38*, L06602. https://doi.org/10.1029/2010GL046573

Davies, M. H., Mix, A. C., Stoner, J. S., Addison, J. A., Jaeger, J., Finney, B., & Wiest, J. (2011). The deglacial transition on the southeastern Alaska Margin: Meltwater input, sea level rise, marine productivity, and sedimentary anoxia. *Paleoceanography*, *26*, PA2223. https://doi.org/10.1029/2010PA002051

De Boer, A. M., & Nof, D. (2004). The exhaust valve of the North Atlantic. *Journal of Climate*, *17*(3), 417–422.

Dumond, D. E., & Griffin, D. G. (2002). Measurements of the marine reservoir effect on radiocarbon ages in the eastern Bering Sea. *Arctic*, 77–86.

Eberl, D. (2004). Quantitative mineralogy of the Yukon River system: Changes with reach and season, and determining sediment provenance. *American Mineralogist*, *89*(11–12), 1784–1794.

Elias, S. A., Short, S. K., Nelson, C. H., & Birks, H. H. (1996). Life and times of the Bering land bridge. *Nature*, *382*(6586), 60–63.

Expedition 323 Scientists (2011). Site U1345. In K. Takahashi, et al. (Eds.), *Proc. IODP, 323 (Integrated Ocean Drilling Program Management International, Inc.)* (pp. 2–4). Tokyo. https://doi.org/10.2204/iodp.proc.323.109.2011

Fairbanks, R. G. (1989). A 17,000-year glacio-eustatic sea level record: influence of glacial melting rates on the Younger Dryas event and deep-ocean circulation. *Nature*, *342*(6250), 637–642.

Fontugne, M. R., & Jouanneau, J.-M. (1987). Modulation of the particulate organic carbon flux to the ocean by a macrotidal estuary: Evidence from measurements of carbon isotopes in organic matter from the Gironde system. *Estuarine, Coastal and Shelf Science*, *24*(3), 377–387.

Ganeshram, R. S., & Pedersen, T. F. (1998). Glacial–interglacial variability in upwelling and bioproductivity off NW Mexico: Implications for Quaternary paleoclimate. *Paleoceanography*, *13*(6), 634–645. https://doi.org/10.1029/98PA02508

Gardner, J. V., Dean, W. E., & Dartnell, P. (1997). Biogenic sedimentation beneath the California Current system for the past 30 kyr and its paleoceanographic significance. *Paleoceanography*, *12*(2), 207–225. https://doi.org/10.1029/96PA03567

Goosse, H., Campin, J., Fichefet, T., & Deleersnijder, E. (1997). Sensitivity of a global ice–ocean model to the Bering Strait throughflow. *Climate Dynamics*, *13*(5), 349–358.

Gorbarenko, S. A. (1996). Stable isotope and lithologic evidence of late-glacial and Holocene oceanography of the northwestern Pacific and its marginal seas. *Quaternary Research*, *46*(3), 230–250.

Gorbarenko, S. A., Artemova, A. V., Goldberg, E. L., & Vasilenko, Y. P. (2014). The response of the Okhotsk Sea environment to the orbital-millennium global climate changes during the Last Glacial Maximum, deglaciation and Holocene. *Global and Planetary Change*, *116*, 76–90. https://doi.org/10.1016/j.gloplacha.2014.02.002

Gorbarenko, S. A., Basov, I. A., Chekhovskaya, M. P., Southon, J., Khusid, T. A., & Artemova, A. V. (2005). Orbital and millennium scale environmental changes in the southern Bering Sea during the last glacial-Holocene: Geochemical and paleontological evidence. *Deep Sea Research Part II: Topical Studies in Oceanography*, *52*, 2174–2185. https://doi.org/10.1016/j.dsr2.2005.08.005

Grebmeier, J. M., McRoy, C. P., & Feder, H. M. (1988). Pelagic-benthic coupling on the shelf of the northern Bering and Chukchi seas. I. Food supply source and benthic biomass. *Marine Ecology Progress Series. Oldendorf*, *48*(1), 57–67.

Gualtieri, L., Glushkova, O., & Brigham-Grette, J. (2000). Evidence for restricted ice extent during the last glacial maximum in the Koryak Mountains of Chukotka, far eastern Russia. *Geological Society of America Bulletin*, *112*(7), 1106–1118. https://doi.org/10.1130/0016-7606(2000)112%C2%A0%3C%C2%A01106:EFRIED%3E2.0.CO;2

Guo, L., & Macdonald, R. W. (2006). Source and transport of terrigenous organic matter in the upper Yukon River: Evidence from isotope (δ^{13}C, Δ^{14}C, and δ^{15}N) composition of dissolved, colloidal, and particulate phases. *Global Biogeochemical Cycles*, *20*, GB2011. https://doi.org/10.1029/2005GB002593

Hans Nelson, C., Baraza, J., & Maldonado, A. (1993). Mediterranean undercurrent sandy contourites, Gulf of Cadiz, Spain. *Sedimentary Geology*, *82*(1), 103–131.

Harvey, G. R. (1980). A study of the chemistry of iodine and bromine in marine sediments. *Marine Chemistry*, *8*(4), 327–332.

Hedges, J. I., & Parker, P. L. (1976). Land-derived organic matter in surface sediments from the Gulf of Mexico. *Geochimica et Cosmochimica Acta*, *40*(9), 1019–1029.

Hendy, I. L., & Kennett, J. P. (2003). Tropical forcing of North Pacific intermediate water distribution during Late Quaternary rapid climate change? *Quaternary Science Reviews*, *22*(5), 673–689.

Hendy, I. L., & Pedersen, T. F. (2005). Is pore water oxygen content decoupled from productivity on the California Margin? Trace element results from Ocean Drilling Program Hole 1017E, San Lucia slope, California. *Paleoceanography*, *20*, PA4026. https://doi.org/10.1029/2004PA001123

Hopkins, D. M. (1959). Cenozoic History of the Bering Land Bridge: The seaway between the Pacific and Arctic basins has often been a land route between Siberia and Alaska. *Science*, *129*(3362), 1519–1528.

Hopkins, D. M. (1979). Landscape and climate of Beringia during late Pleistocene and Holocene time. *The First Americans: Origins, Affinities and Adaptations*, *15*, 42.

Hopkins, D. M. (1982). Aspects of the paleogeography of Beringia during the late Pleistocene. In D. M. Hopkins, et al. (Eds.), *Paleoecology of Beringia* (pp. 3–28). New York: Academic Press.

Hu, A., & Meehl, G. A. (2005). Bering Strait throughflow and the thermohaline circulation. *Geophysical Research Letters*, *32*, L24610. https://doi.org/10.1029/2005GL024424

Hu, A., Meehl, G. A., Han, W., Otto-Bliestner, B., Abe-Ouchi, A., & Rosenbloom, N. (2014). Effects of the Bering Strait closure on AMOC and global climate under different background climates. *Progress in Oceanography*, *132*, 174–196. https://doi.org/10.1016/j.pocean.2014.02.004

Hurst, M. P., Aguilar-Islas, A. M., & Bruland, K. W. (2010). Iron in the southeastern Bering Sea: Elevated leachable particulate Fe in shelf bottom waters as an important source for surface waters. *Continental Shelf Research*, *30*, 467–480. https://doi.org/10.1016/j.csr.2010.01.001

Intergovernmental Panel on Climate Change (2013). In T. F. Stocker, et al. (Eds.), *IPCC, 2013: Climate Change 2013: The Physical Science Basis. Contribution of Working Group I to the Fifth Assessment Report of the Intergovernmental Panel on Climate Change* (p. 1535). Cambridge, UK: Cambridge University Press. https://doi.org/10.1017/CBO9781107415324

Ishizaki, Y., Ohkushi, K., Ito, T., & Kawahata, H. (2009). Abrupt changes of intermediate-water oxygen in the northwestern Pacific during the last 27 kyr. *Geo-Marine Letters*, *29*(2), 125–131.

Itaki, T., Uchida, M., Kim, S., Shin, H.-S., Tada, R., & Khim, B.-K. (2009). Late Pleistocene stratigraphy and palaeoceanographic implications in northern Bering Sea slope sediments: Evidence from the radiolarian species *Cycladophora davisiana*. *Journal of Quaternary Science*, *24*, 856–865. https://doi.org/10.1002/jqs.1356

Jakobsson, M., Pearce, C., Cronin, T. M., Backman, J., Anderson, L. G., Barrientos, N., … Mayer, L. A. (2017). Post-glacial flooding of the Bering Land Bridge dated to 11 cal ka BP based on new geophysical and sediment records. *Climate of the Past*, *13*(8), 991.

Johnson, G. C., Stabeno, P. J., & Riser, S. C. (2004). The Bering slope current system revisited. *Journal of Physical Oceanography*, *34*, 384–398.

Kao, S., Liu, K., Hsu, S., Chang, Y., & Dai, M. (2008). North Pacific-wide spreading of isotopically heavy nitrogen during the last deglaciation: Evidence from the western Pacific. *Biogeosciences*, *5*, 1641–1650.

Katsuki, K., & Takahashi, K. (2005). Diatoms as paleoenvironmental proxies for seasonal productivity, sea-ice and surface circulation in the Bering Sea during the late Quaternary. *Deep Sea Research Part II: Topical Studies in Oceanography*, *52*, 2110–2130. https://doi.org/10.1016/j.dsr2.2005.07.001

Keigwin, L. D. (2002). Late Pleistocene-Holocene paleoceanography and ventilation of the Gulf of California. *Journal of Oceanography*, *58*(2), 421–432.

Keigwin, L. D., Donnelly, J. P., Cook, M. S., Driscoll, N. W., & Brigham-Grette, J. (2006). Rapid sea-level rise and Holocene climate in the Chukchi Sea. *Geology*, *34*, 861. https://doi.org/10.1130/G22712.1

Keigwin, L. D., Jones, G., & Froelich, P. (1992). A 15,000 year paleoenvironmental record from Meiji Seamount, far northwestern Pacific. *Earth and Planetary Science Letters*, *111*(2), 425–440.

Keigwin, L. D., Jones, G. A., Lehman, S. J., & Boyle, E. A. (1991). Deglacial meltwater discharge, North Atlantic deep circulation, and abrupt climate change. *Journal of Geophysical Research*, *96*(C9), 16,811–16,826. https://doi.org/10.1029/91JC01624

Kennett, J. P., & Ingram, B. L. (1995). A 20,000-year record of ocean circulation and climate change from the Santa Barbara basin. *Nature*, *377*, 510–514.

Khim, B.-K., Kim, S., Uchida, M., & Itaki, T. (2011). High organic carbon deposition in the northern margin of the Aleutian Basin (Bering Sea) before the last deglaciation. *Ocean Science Journal*, *45*, 203–211. https://doi.org/10.1007/s12601-010-0019-y

Kim, S., Khim, B. K., Uchida, M., Itaki, T., & Tada, R. (2011). Millennial-scale paleoceanographic events and implication for the intermediate-water ventilation in the northern slope area of the Bering Sea during the last 71 kyr. *Global and Planetary Change*, *79*(1–2), 89–98. https://doi.org/10.1016/j.gloplacha.2011.08.004

Kinder, T., Coachman, L., & Galt, J. (1975). The Bering slope current system. *Journal of Physical Oceanography*, *5*(2), 231–244.

Kinney, C. J., Maslowski, W., & Okkonen, S. (2009). On the processes controlling shelf–basin exchange and outer shelf dynamics in the Bering Sea. *Deep Sea Research Part II: Topical Studies in Oceanography*, *56*, 1351–1362. https://doi.org/10.1016/j.dsr2.2008.10.023

Kohfeld, K. E., & Chase, Z. (2011). Controls on deglacial changes in biogenic fluxes in the North Pacific Ocean. *Quaternary Science Reviews*, *30*, 3350–3363. https://doi.org/10.1016/j.quascirev.2011.08.007

Kuehn, H., Lembke-Jene, L., Gersonde, R., Esper, O., Lamry, F., Arz, H., & Tiedemann, R. (2014). Laminated sediments in the Bering Sea reveal atmospheric teleconnections to Greenland climate on millennial to decadal timescales during the last deglaciation. *Climate of the Past*, 2467–2518. https://doi.org/10.5194/cpd-10-2467-2014

Kuzmin, Y. V., Burr, G. S., & Jull, A. T. (2001). Radiocarbon reservoir correction ages in the Peter the Great Gulf, Sea of Japan, and eastern coast of the Kunashir, southern Kuriles (northwestern Pacific). *Radiocarbon*, *43*(2), 477–482.

Lam, P. J., Robinson, L. F., Blusztajn, J., Li, C., Cook, M. S., McManus, J. F., & Keigwin, L. D. (2013). Transient stratification as the cause of the North Pacific productivity spike during deglaciation. *Nature Geoscience*, *6*(8), 622–626. https://doi.org/10.1038/ngeo1873

Lambeck, K., Rouby, H., Purcell, A., Sun, Y., & Sambridge, M. (2014). Sea level and global ice volumes from the Last Glacial Maximum to the Holocene. *Proceedings of the National Academy of Sciences of the United States of America*, *111*(43), 15,296–15,303.

Lehman, S. I., & Keigwin, L. D. (1992). Sudden changes in North Atlantic circulation during the last deglaciation. *Nature*, *356*, 757.

Lehmann, M. F., Sigman, D. M., McCorkle, D. C., Brunelle, B. G., Hoffmann, S., Kienast, M., … Clement, J. (2005). Origin of the deep Bering Sea nitrate deficit: Constraints from the nitrogen and oxygen isotopic composition of water column nitrate and benthic nitrate fluxes. *Global Biogeochemical Cycles*, *19*, GB4005. https://doi.org/10.1029/2005GB002508

Leri, A. C., Mayer, L. M., Thornton, K. R., Northrup, P. A., Dunigan, M. R., Ness, K. J., & Gellis, A. B. (2015). A marine sink for chlorine in natural organic matter. *Nature Geoscience*, *8*(8), 620–624.

Lobbes, J. M., Fitznar, H. P., & Kattner, G. (2000). Biogeochemical characteristics of dissolved and particulate organic matter in Russian rivers entering the Arctic Ocean. *Geochimica et Cosmochimica Acta*, *64*(17), 2973–2983.

Löwemark, L., Jakobsson, M., Mrth, M., & Backman, J. (2008). Arctic Ocean manganese contents and sediment colour cycles. *Polar Research*, *27*, 105–113. https://doi.org/10.1111/j.1751-8369.2008.00055.x

Mangerud, J., Andersen, S. T., Berglund, B. E., & Donner, J. J. (1974). Quaternary stratigraphy of Norden, a proposal for terminology and classification. *Boreas*, *3*(3), 109–126.

Mann, D. H., & Hamilton, T. D. (1995). Late Pleistocene and Holocene paleoenvironments of the North Pacific coast. *Quaternary Science Reviews*, *14*(5), 449–471.

MathWorks. (2014). MATLAB (Version R2014a). MathWorks. Retrieved from http://www.mathworks.com/products/matlab/

Max, L., Lembke-Jene, L., Riethdorf, J.-R., Tiedemann, R., Nürnberg, D., Kühn, H., & Mackensen, A. (2014). Pulses of enhanced North Pacific Intermediate Water ventilation from the Okhotsk Sea and Bering Sea during the last deglaciation. *Climate of the Past*, *10*(2), 591–605. https://doi.org/10.5194/cp-10-591-2014

McManus, J. F., Francois, R., Gherardi, J.-M., Keigwin, L. D., & Brown-Leger, S. (2004). Collapse and rapid resumption of Atlantic meridional circulation linked to deglacial climate changes. *Nature*, *428*(6985), 834–837.

McManus, D. A., Venkatarathnam, K., Hopkins, D. M., & Nelson, C. H. (1974). Yukon River sediment on the northernmost Bering Sea shelf. *Journal of Sedimentary Research*, *44*(4), 1052–1060. https://doi.org/10.1306/212F6C2B-2B24-11D7-8648000102C1865D

McNeely, R., Dyke, A. S., & Southon, J. R. (2006). *Canadian marine reservoir ages, preliminary data assessment, Open File 5049*. Geological Survey Canada.

Meyer, V. D., Hefter, J., Lohmann, G., Max, L., Tiedemann, R., & Mollenhauer, G. (2017). Summer temperature evolution on the Kamchatka Peninsula, Russian Far East, during the past 20 000 years. *Climate of the Past*, *13*(4), 359.

Meyers, P. A. (1994). Preservation of elemental and isotopic source identification of sedimentary organic matter. *Chemical Geology*, *114*(3), 289–302.

Mikolajewicz, U., Crowley, T. J., Schiller, A., & Voss, R. (1997). Modeling teleconnections between the North Atlantic and North Pacific during the Younger Dryas. *Nature*, *387*(6631), 384–387.

Misarti, N., Finney, B. P., Jordan, J. W., Maschner, H. D. G., Addison, J. A., Shapley, M. D., … Beget, J. E. (2012). Early retreat of the Alaska Peninsula Glacier Complex and the implications for coastal migrations of First Americans. *Quaternary Science Reviews*, *48*, 1–6. https://doi.org/10.1016/j.quascirev.2012.05.014

Mix, A. C., Lund, D. C., Pisias, N. G., Bodén, P., Bornmalm, L., Lyle, M., & Pike, J. (1999). Rapid climate oscillations in the northeast Pacific during the last deglaciation reflect Northern and Southern Hemisphere sources. *Geophysical Monograph Series*, *112*, 127–148.

Nagashima, K., Asahara, Y., Takeuchi, F., Harada, N., Toyoda, S., & Tada, R. (2012). Contribution of detrital materials from the Yukon River to the continental shelf sediments of the Bering Sea based on the electron spin resonance signal intensity and crystallinity of quartz. *Deep Sea Research Part II: Topical Studies in Oceanography*, *61–64*, 145–154. https://doi.org/10.1016/j.dsr2.2011.12.001

Naidu, A. S., Cooper, L. W., Finney, B. P., Macdonald, R. W., Alexander, C., & Semiletov, I. P. (2000). Organic carbon isotope ratios (δ^{13}C) of Arctic Amerasian Continental shelf sediments. *International Journal of Earth Sciences*, *89*(3), 522–532. https://doi.org/10.1007/s005310000121

Naidu, A. S., Cooper, L., Grebmeier, J., Whitledge, T., & Hameedi, M. (2004). The continental margin of the North Bering-Chukchi Sea: Concentrations, sources, fluxes, accumulation and burial rates of organic carbon. In *The Organic Carbon Cycle in the Arctic Ocean* (pp. 193–203). Berlin: Springer.

Naidu, A. S., Scalan, R. S., Feder, H. M., Goering, J. J., Hameedi, M. J., Parker, P. L., … Jewett, S. C. (1993). Stable organic carbon isotopes in sediments of the north Bering-south Chukchi seas, Alaskan-Soviet Arctic Shelf. *Continental Shelf Research*, *13*(5–6), 669–691. https://doi.org/10.1016/0278-4343(93)90099-J

Nakatsuka, T., Watanabe, K., Handa, N., Matsumoto, E., & Wada, E. (1995). Glacial to interglacial surface nutrient variations of Bering deep basins recorded by δ^{13}C and δ^{15}N of sedimentary organic matter. *Paleoceanography*, *10*(6), 1047–1061. https://doi.org/10.1029/95PA02644

Obata, A., Ishizaka, J., & Endoh, M. (1996). Global verification of critical depth theory for phytoplankton bloom with climatological in situ temperature and satellite ocean color data. *Journal of Geophysical Research: Oceans*, *101*(C9), 20,657–20,667.

Okazaki, Y., Kimoto, K., Asahi, H., Sato, M., Nakamura, Y., & Harada, N. (2014). Glacial to deglacial ventilation and productivity changes in the southern Okhotsk Sea. *Paleogeography, Palaeoclimatology, Palaeoecology*, *395*, 53–66. https://doi.org/10.1016/j.palaeo.2013.12.013

Okazaki, Y., Takahashi, K., Asahi, H., Katsuki, K., Hori, J., Yasuda, H., … Tokuyama, H. (2005). Productivity changes in the Bering Sea during the late Quaternary. *Deep Sea Research Part II: Topical Studies in Oceanography*, *52*, 2150–2162. https://doi.org/10.1016/j.dsr2.2005.07.003

Okazaki, Y., Timmermann, A., Menviel, L., Harada, N., Abe-Ouchi, A., Chikamoto, M. O., … Asahi, H. (2010). Deepwater formation in the North Pacific during the last glacial termination. *Science*, *329*, 200–204. https://doi.org/10.1126/science.1190612

Okkonen, S. R., Schmidt, G. M., Cokelet, E. D., & Stabeno, P. J. (2004). Satellite and hydrographic observations of the Bering Sea "Green Belt". *Deep Sea Research Part II: Topical Studies in Oceanography*, *51*, 1033–1051. https://doi.org/10.1016/j.dsr2.2003.08.005

Otosaka, S., Honda, M. C., & Noriki, S. (2004). La/Yb and Th/Sc in settling particles: Vertical and horizontal transport of lithogenic material in the western North Pacific. *Geochemical Journal*, *38*(6), 515–525.

Overland, J. E., & Pease, C. H. (1982). Cyclone climatology of the Bering Sea and its relation to sea ice extent. *Monthly Weather Review*, *110*(1), 5–13. https://doi.org/10.1175/1520-0493(1982)110%C2%A0%3C%C2%A00005:CCOTBS%3E2.0.CO;2

Peltier, W. R., & Fairbanks, R. G. (2006). Global glacial ice volume and Last Glacial Maximum duration from an extended Barbados sea level record. *Quaternary Science Reviews*, *25*, 3322–3337. https://doi.org/10.1016/j.quascirev.2006.04.010

Prahl, F., Ertel, J., Goni, M., Sparrow, M., & Eversmeyer, B. (1994). Terrestrial organic carbon contributions to sediments on the Washington margin. *Geochimica et Cosmochimica Acta*, *58*(14), 3035–3048.

Price, N., & Calvert, S. (1977). The contrasting geochemical behaviours of iodine and bromine in recent sediments from the Namibian shelf. *Geochimica et Cosmochimica Acta*, *41*(12), 1769–1775.

Ramnarine, R., Voroney, R. P., Wagner-Riddle, C., & Dunfield, K. E. (2011). Carbonate removal by acid fumigation for measuring the $\delta^{13}C$ of soil organic carbon. *Canadian Journal of Soil Science*, *91*, 247–250. https://doi.org/10.4141/cjss10066

Rasmussen, S. O., Andersen, K. K., Svensson, A. M., Steffensen, J. P., Vinther, B. M., Clausen, H. B., … Ruth, U. (2006). A new Greenland ice core chronology for the last glacial termination. *Journal of Geophysical Research*, *111*, D06102. https://doi.org/10.1029/2005JD006079

Ratnayake, N. P., Suzuki, N., & Matsubara, M. (2005). Sources of long chain fatty acids in deep sea sediments from the Bering Sea and the North Pacific Ocean. *Organic Geochemistry*, *36*, 531–541. https://doi.org/10.1016/j.orggeochem.2004.11.004

Ratnayake, N. P., Suzuki, N., Okada, M., & Takagi, M. (2006). The variations of stable carbon isotope ratio of land plant-derived n-alkanes in deep-sea sediments from the Bering Sea and the North Pacific Ocean during the last 250,000 years. *Chemical Geology*, *228*, 197–208. https://doi.org/10.1016/j.chemgeo.2005.10.005

Reimer, P. J., Bard, E., Bayliss, A., Beck, J. W., Blackwell, P. G., Ramsey, C. B., … Friedrich, M. (2013). IntCal13 and Marine13 radiocarbon age calibration curves 0–50,000 years cal BP. *Radiocarbon*, *55*(4), 1869–1887.

Riethdorf, J., Max, L., Nürnberg, D., Lembke-Jene, L., & Tiedemann, R. (2013). Deglacial development of (sub) sea surface temperature and salinity in the subarctic northwest Pacific: Implications for upper-ocean stratification. *Paleoceanography*, *28*, 91–104. https://doi.org/10.1002/palo.20014

Roach, A. T., Aagaard, K., Pease, C. H., Salo, S. A., Weingartner, T., Pavlov, V., & Kulakov, M. (1995). Direct measurements of transport and water properties through the Bering Strait. *Journal of Geophysical Research*, *100*(C9), 18,443–18,457. https://doi.org/10.1029/95JC01673

Sambrotto, R., Goering, J., & McRoy, C. (1984). Large yearly production of phytoplankton in the western Bering Strait. *Science*, *225*(4667), 1147–1150.

Sancetta, C. (1995). Diatoms in the Gulf of California: Seasonal flux patterns and the sediment record for the last 15,000 years. *Paleoceanography*, *10*(1), 67–84. https://doi.org/10.1029/94PA02796

Sancetta, C., Heusser, L., Labeyrie, L., Naidu, A. S., & Robinson, S. W. (1985). Wisconsin—Holocene paleoenvironment of the Bering Sea: Evidence from diatoms, pollen, oxygen isotopes and clay minerals. *Marine Geology*, *62*(1), 55–68.

Sarnthein, M., Grootes, P. M., Kennett, J. P., & Nadeau, M.-J. (2007). 14C reservoir ages show deglacial changes in ocean currents and carbon cycle. In A. Schmittner, J. C. H. Chiang, & S. R. Hemming (Eds.), *Ocean circulation: Mechanisms and impacts — Past and future changes of meridional overturning, Geophysical Monograph Series* (Vol. 173, pp. 175–196). Washington, DC: American Geophysical Union.

Schlung, S. A., Christina Ravelo, A., Aiello, I. W., Andreasen, D. H., Cook, M. S., Drake, M., … Takahashi, K. (2013). Millennial-scale climate change and intermediate water circulation in the Bering Sea from 90 ka: A high-resolution record from IODP Site U1340. *Paleoceanography*, *28*, 54–67. https://doi.org/10.1029/2012PA002365

Schubert, C. J., & Calvert, S. E. (2001). Nitrogen and carbon isotopic composition of marine and terrestrial organic matter in Arctic Ocean sediments: implications for nutrient utilization and organic matter composition. *Deep Sea Research Part I: Oceanographic Research Papers*, *48*(3), 789–810. https://doi.org/10.1016/S0967-0637(00)00069-8

Schumacher, J., & Reed, R. (1992). Characteristics of currents over the continental slope of the eastern Bering Sea. *Journal of Geophysical Research*, *97*(C6), 9423–9433.

Schumacher, J., & Stabeno, P. J. (1998). The continental shelf of the Bering Sea. In A. R. Robinson & K. H. Brink (Eds.), *The Sea: The Global Coastal Ocean Regional Studies and Synthesis* (Vol. 11, pp. 869–909). New York: John Wiley.

Shaffer, G. (1994). Role of the Bering Strait in controlling North Atlantic. *Nature*, *367*(6461), 354–357.

Shibahara, A., Ohkushi, K., Kennett, J. P., & Ikehara, K. (2007). Late Quaternary changes in intermediate water oxygenation and oxygen minimum zone, northern Japan: A benthic foraminiferal perspective. *Paleoceanography*, *22*, PA3213. https://doi.org/10.1029/2005PA001234

Shultz, D. J., & Calder, J. A. (1976). Organic carbon $^{13}C/^{12}C$ variations in estuarine sediments. *Geochimica et Cosmochimica Acta*, *40*(4), 381–385.

Sigman, D. M., Casciotti, K. L., Andreani, M., Barford, C., Galanter, M., & Böhlke, J. (2001). A bacterial method for the nitrogen isotopic analysis of nitrate in seawater and freshwater. *Analytical Chemistry*, *73*(17), 4145–4153.

Sigman, D. M., Karsh, K., & Casciotti, K. (2009). Ocean process tracers: nitrogen isotopes in the ocean. *Encyclopedia of Ocean Science*, 4138–4153.

Springer, A. M., McRoy, C. P., & Flint, M. V. (1996). The Bering Sea Green Belt: Shelf-edge processes and ecosystem production. *Fisheries Oceanography*, *5*(3-4), 205–223.

Springer, A. M., McRoy, C. P., & Turco, K. R. (1989). The paradox of pelagic food webs in the northern Bering Sea—II. Zooplankton communities. *Continental Shelf Research*, *9*(4), 359–386.

Stabeno, P. J., Schumacher, J. D., & Ohtani, K. (1999). The physical oceanography of the Bering Sea. *Dynamics of the Bering Sea*, 1–28.

Stein, R. (1986). Organic carbon and sedimentation rate—Further evidence for anoxic deep-water conditions in the Cenomanian/Turonian Atlantic Ocean. *Marine Geology*, *72*(3), 199–209.

Stein, R., & Macdonald, R. (2004). Geochemical proxies used for organic carbon source identification in Arctic Ocean sediments. In R. Stein & R. W. Macdonald (Eds.), *The Organic Carbon Cycle in the Arctic Ocean* (pp. 24–32). Berlin: Springer.

Sverdrup, H. (1953). On conditions for the vernal blooming of phytoplankton. *Journal du Conseil*, *18*(3), 287–295.

Takahashi, K. (1998). The Bering and Okhotsk Seas: Modern and past paleoceanographic changes and gateway impact. *Journal of Asian Earth Sciences*, *16*(1), 49–58.

Tarasov, L., & Peltier, W. R. (2005). Arctic freshwater forcing of the Younger Dryas cold reversal. *Nature*, *435*, 662–665. https://doi.org/10.1038/nature03617

Trefry, J. H., Trocine, R. P., Cooper, L. W., & Dunton, K. H. (2014). Trace metals and organic carbon in sediments of the northeastern Chukchi Sea. *Deep Sea Research Part II: Topical Studies in Oceanography*, *102*, 18–31. https://doi.org/10.1016/j.dsr2.2013.07.018

Tremblay, J.-É., Anderson, L. G., Matrai, P., Coupel, P., Bélanger, S., Michel, C., & Reigstad, M. (2015). Global and regional drivers of nutrient supply, primary production and CO_2 drawdown in the changing Arctic Ocean. *Progress in Oceanography*, *139*, 171–196.

Van der Plicht, J., Van Geel, B., Bohncke, S., Bos, J., Blaauw, M., Speranza, A., … Björck, S. (2004). The Preboreal climate reversal and a subsequent solar-forced climate shift. *Journal of Quaternary Science*, *19*, 263–269.

Viscosi-Shirley, C., Pisias, N., & Mammone, K. (2003). Sediment source strength, transport pathways and accumulation patterns on the Siberian–Arctic's Chukchi and Laptev shelves. *Continental Shelf Research*, *23*(11–13), 1201–1225. https://doi.org/10.1016/S0278-4343(03)00090-6

Waelbroeck, C., Labeyrie, L., Michel, E., Duplessy, J. C., McManus, J., Lambeck, K., … Labracherie, M. (2002). Sea-level and deep water temperature changes derived from benthic foraminifera isotopic records. *Quaternary Science Reviews*, *21*(1), 295–305.

Walsh, J., McRoy, C., Coachman, L., Goering, J., Nihoul, J., Whitledge, T., … Shuert, P. (1989). Carbon and nitrogen cycling within the Bering/Chukchi Seas: Source regions for organic matter effecting AOU demands of the Arctic Ocean. *Progress in Oceanography*, *22*(4), 277–359.

Weaver, A. J. (2003). Meltwater Pulse 1A from Antarctica as a Trigger of the Bolling-Allerod Warm Interval. *Science*, *299*(5613), 1709–1713. https://doi.org/10.1126/science.1081002

Wentworth, C. K. (1922). A scale of grade and class terms for clastic sediments. *The Journal of Geology*, 377–392.

Zheng, Y., Geen, A., Anderson, R. F., Gardner, J. V., & Dean, W. E. (2000). Intensification of the Northeast Pacific oxygen minimum zone during the Bølling-Allerød Warm Period. *Paleoceanography*, *15*(5), 528–536. https://doi.org/10.1029/2003PA000979

Ziegler, M., Jilbert, T., de Lange, G. J., Lourens, L. J., & Reichart, G.-J. (2008). Bromine counts from XRF scanning as an estimate of the marine organic carbon content of sediment cores. *Geochemistry, Geophysics, Geosystems*, *9*, Q05009. https://doi.org/10.1029/2007GC001932